This is a preprint, the final version is subject to change, of the American Mineralogist (MSA)
Cite as Authors (Year) Title. American Mineralogist, in press.
DOI: http://dx.doi.org/10.2138/am-2018-6210

REVISION 1

EXPERIMENTAL CALIBRATION AND IMPLICATIONS OF OLIVINE-MELT VANADIUM OXYBAROMETRY FOR HYDROUS BASALTIC ARC MAGMAS

Shishkina T.A.[1,2*], Portnyagin M.V.[1,3], Botcharnikov R.E.[2,4], Almeev R.R.[2], Simonyan A.V.[2], Garbe-Schönberg, D.[5], Schuth, S.[2], Oeser, M.[2] and Holtz F.[2]

* t.shishkina@geokhi.ru

1 - V.I. Vernadsky Institute of Geochemistry and Analytical Chemistry, Kosygin str. 19, 119191, Moscow, Russia, t.shishkina@geokhi.ru, +7-925-053-49-71

2 - Institute für Mineralogie, Leibniz Universität Hannover, Callinstr, 3, 30167 Hannover, Germany

3 - GEOMAR Helmholtz Centre for Ocean Research Kiel, Wischhofstrasse 1-3, 24148 Kiel, Germany

4 - Institute für Geowissenschaften, Johannes Gutenberg Universität Mainz , J.-J.-Becher-Weg 21, 55128 Mainz, Germany

5 - Institute of Geosciences, Christian-Albrechts University of Kiel, Ludewig-Meyn-Strasse 10, 24118 Kiel, Germany

ABSTRACT

The strong dependence of vanadium partitioning between olivine and silicate melt (D_V^{Ol-M}) on redox conditions (fO_2) can be used as sensitive oxybarometer in magmatic systems. Here we extend the experimental database on D_V^{Ol-M}, obtained so far at high temperatures (mainly above 1250°C), to lower temperatures which are typical for island-arc basalts. Crystallization experiments were performed using a composition from Mutnovsky volcano (Kamchatka), and

the investigated temperature, pressure and oxygen fugacity ranges were 1025-1150°C, 0.1 and 0.3 GPa and ΔQFM of -0.5 to +3.2, respectively. The water content in melts ranged from 0.6 to ~6.5 wt.% H_2O. The data demonstrate a strong negative correlation between $D_V^{Ol\text{-}M}$ and oxygen fugacity, similar to the behavior observed previously at higher temperatures and in MgO-rich compositions. The correlation between $D_V^{Ol\text{-}M}$ and ΔQFM in the range from -0.5 to +3.2 is described for melts with MgO<12 wt.% and Na_2O<4 wt.% at temperatures ≤ 1250°C by the empirical equation: $\Delta\,\mathrm{QFM} = -3.07^{+0.26}_{-0.29}\log D_V^{Ol-M} - 3.34^{+0.40}_{-0.49}$ with the standard error (SE) as a function of $\log D_V^{Ol-M}$:$2\mathrm{SE}\,(\Delta\mathrm{QFM}) = -0.275\log D_V^{Ol-M} + 0.4$.

We suggest that this equation can be used as an oxybarometer which is particularly well applicable to the hydrous island-arc magmas at relatively low temperature. Application of the equation to the composition of melt inclusions and their host olivine phenocrysts from basalts of Mutnovsky volcano, containing vanadium concentrations in the range of 250-370 ppm and 4-6 ppm, respectively, reveals an oxygen fugacity in the range ΔQFM +1.9 to +2.3. The estimates are in a good agreement with olivine-spinel oxybarometry for Mutnovsky basalts and may be typical for moderately evolved island-arc magmas.

Key words: vanadium, oxybarometry, island arcs, melt inclusions, redox conditions

1. INTRODUCTION

Redox conditions of the origin and evolution of subduction-related magmas remain to be one the most controversial issues in magmatic petrology (e.g., Carmichael, 1991; Parkinson and Arculus, 1999; Evans, 2012). Some studies argue that sub-arc primary magmas derive from the mantle wedge at more oxidized conditions in comparison to mid-ocean ridge environments as a result of mantle oxidation by slab-derived components, containing H_2O, sulphur and/or ferric

iron (e.g., Parkinson and Arculus, 1999; Mungall, 2002; Kelley and Cottrell, 2009; Brounce et al., 2014). On the other hand the studies of redox-sensitive element ratios (like V/Sc, V/Ga or Zn/Fe) in primitive rocks have been interpreted to reflect no significant difference between the mantle oxidation state at subduction zones and ocean ridges (e.g., Lee et al., 2005; 2010; Mallmann and O`Neill, 2009; Laubier et al., 2014). The redox conditions in the course of magma differentiation also have contradictory estimations. Some studies suggested that island-arc magmas formed at shallower levels are more oxidized due to differentiation and/or interaction with preexisting crust (e.g., Lee et al., 2005; 2012). On the other hand, recent investigations using X-ray absorption near-edge structure (XANES) spectroscopy at the iron and sulphur K-edges in quenched glasses and melt inclusions from different localities in subduction and intraplate setting have shown no significant magma oxidation or even strong Fe and S reduction during magma ascent and associated degassing (Kelley and Cottrell, 2012; Brounce et al., 2014; 2016; 2017; Moussallam et al., 2014). The redox state of primary island-arc magmas as well as magmas evolving in the crust thus remains controversial and requires further investigations using alternative methodological approaches.

One of the perspective methods proposed to quantify the redox conditions in magmatic systems is based on the dependence of vanadium partitioning between Mg-Fe silicates (olivine, pyroxene) and coexisting silicate melt on oxygen fugacity. Vanadium is a multivalent element with the possible valence states of +2, +3, +4, and +5, and the states of +3 and +4 prevail in natural magmatic systems (Borisov et al., 1987). Both V species have similar ionic radii in octahedral coordination (Shannon, 1976). However, V^{3+} has been shown to be more compatible in Fe-Mg silicates compared to V^{4+}, which is likely due to the easier charge balance (Canil and Fedortchouk, 2001; Papike et al., 2005). Rising oxygen fugacity (fO_2) leads to the increase of V^{4+}/V^{3+} ratio in melt and therefore influences the V partitioning coefficient between Fe-Mg silicates and melt. Hence D_V dependence on fO_2 can be used as oxybarometer, provided that it

is calibrated experimentally. The main advantage of the "V-in-olivine oxybarometer" is the possibility to estimate redox conditions for rocks which do not contain spinel as a liquidus phase (i.e., komatiites, Canil, 1997), when the commonly used olivine-spinel (±orthopyroxene) oxybarometry (e.g., Ballhaus et al., 1991) cannot be applied. A further advantage is a weak dependence of V partitioning on temperature, pressure and melt composition (Canil and Fedortchouk, 2001; Mallmann and O'Neill, 2013).

A number of published experimental studies present data of vanadium partitioning between olivine and silicate melt depending on oxygen fugacity in mafic and ultramafic systems, and the presently available experimental dataset includes about 300 compositions (e.g., Gaetani and Grove, 1997; Canil, 1997; Canil and Fedortchouk, 2001; Shearer et al., 2006; Mallmann and O'Neill, 2009; 2013; Tuff and O'Neill, 2010; Papike et al., 2013; Laubier et al., 2014) (Fig. 1A, B). These partitioning experiments were performed for a variety of starting melt compositions including komatiites, primitive Martian basalt, barred olivine chondrule, mid-ocean ridge basalts (MORBs), Hawaiian tholeiitic basalt, basaltic andesite and synthetic compositions in CMAS and FCMAS systems. The majority of experimental data are for MgO-rich (>10 wt%) melts (e.g., komatiites) equilibrated at temperatures above 1250°C (Fig. 1C). Only a few experiments were conducted with magmas containing less than 10 wt.% MgO and at temperatures below 1250°C (Fig. 1 C, D) (e.g., Hawaiian tholeiitic basalt (Canil and Fedortchouk, 2001) and MORB and basaltic andesite (Laubier et al., 2014)). Most of the cited above experiments were conducted at atmospheric pressure with only a few runs conducted at elevated pressures of 0.5 – 2 GPa. All previously published experiments were performed at anhydrous conditions so the potential influence of water on V partitioning has not been studied yet. Most previous experiments were performed at redox conditions of QFM±4 (where QFM is a Quartz-Fayalite-Magnetite oxygen buffer and the numbers refer to the deviation of fO_2 from the buffer expressed in log units), which cover the variety of conditions for natural magmas

(Fig. 1 A, C). An extended range of redox conditions (-13.5<QFM<+10) was investigated by Mallmann and O'Neill (2009) (Fig. 1 A, C).

The scarcity of experiments performed at relatively low temperature conditions and in H_2O-bearing systems limits the reliability of the proposed equations when they are applied to estimate the redox conditions of typical subduction-related magmas, crystallizing at temperatures below 1250°C (e.g., Sobolev and Chaussidon, 1996; Mironov et al., 2015) and containing up to several percent of dissolved H_2O (e.g., Sobolev and Chaussidon, 1996; Wallace, 2005; Portnyagin et al., 2007; Ruscitto et al., 2010). This study presents new experimental data on $D_V^{Ol\text{-}M}$ for natural high-Al island-arc basalt from Mutnovsky volcano (Kamchatka). A strong negative correlation of $D_V^{Ol\text{-}M}$ with ΔQFM is established on the basis of our and previously published experimental data at T≤1250°C. The V-in-olivine oxybarometer, updated for low temperature and hydrous conditions, was used to estimate the redox conditions in the magma reservoir of Mutnovsky volcano using melt inclusions in olivine phenocrysts from natural basaltic tephra and lava samples.

2. EXPERIMENTAL AND ANALYTICAL METHODS

2.1 SAMPLES

The crystallization experiments were performed with a natural high-Al, low-K basalt (sample N72) – a lava of the latest (Late Pleistocene to Holocene) activity of Mutnovsky volcano in the Southern Kamchatka (Selyangin, 1993; Chashchin et al., 2011). The N72 basalt sample has one of the most primitive compositions of this volcano and comprises about 20% plagioclase and olivine phenocrysts (up to 5 mm in size) and a fine-grained groundmass consisting of plagioclase, clinopyroxene and magnetite. The sample represents a common type of basalts in the Kamchatka arc and elsewhere, particularly in subduction-related settings with relatively thin overriding plate (e.g., Plank and Langmuir, 1988; Kelemen et al., 1995). The major and

trace elements concentrations in sample N72 were reported by Duggen et al. (2007). For the experiments, the rock was powdered and melted in a platinum crucible during 3 hours at 1600°C and atmospheric air conditions with subsequent quenching to glass by pouring the melt onto a brass plate. The glass was crushed into small pieces and re-melted again for 1.5 hours at the same conditions with subsequent quenching to glass. The final glass was powdered and split in two fractions of <125 μm and 125–200 μm, which were mixed in 1:1 volume proportion.

2.2 EXPERIMENTAL METHODS

2.2.1 Capsule preparation technique

Experiments at temperatures below 1050°C were performed in Au capsules. At higher temperatures $Au_{80}Pd_{20}$ capsules were used. The capsules were tubes of about 15 mm long with inner diameter of 2.6 mm welded shut from both sides. For water-saturated experiments (series "V" in Table 1), the capsules were filled with 50 mg basaltic glass powder and about 10 wt.% of distilled water to ensure water saturation of the melt. For water-undersaturated experiments (series "N" in Table 1), every capsule was charged with 30-50 mg of basaltic glass powder and various amounts of distilled water and silver oxalate (source of CO_2). The bulk amount of added volatiles was sufficient to reach saturation of the melt with H_2O+CO_2 fluid and the proportions of water and silver oxalate varied to adjust the desired mole fraction of water (XH_2O^{fl}) in the fluid. Previously, this sample was used for an experimental study of the solubility of mixed H_2O-CO_2-bearing fluids in basaltic melt at pressures of 50 to 500 MPa (Shishkina et al., 2010, 2014). Neither Au nor $Au_{80}Pd_{20}$ capsules were pre-saturated with Fe. Iron loss from the melt into the capsule is not observed if Au capsules are used. However, as shown previously for the investigated composition, Fe-loss into the $Au_{80}Pd_{20}$ capsules is below 6 % relative to the initial composition for experiments performed at aH_2O > 0.1 (Shishkina et al., 2010).

2.2.2. Experimental technique

Crystallization experiments with Mutnovsky basalt were performed in a vertically oriented Internally Heated Pressure Vessel (IHPV) with an argon or argon-hydrogen mixture as a pressure medium at the Institut für Mineralogie, Leibniz Universität Hannover, Germany. The detailed description of the experimental equipment and procedure is given elsewhere (Berndt et al., 2002; Botcharnikov et al., 2005). The pressure was continuously monitored with a calibrated Burster Type 8221 digital pressure transducer (pressure uncertainty ±1 MPa). Pressure variations during the experimental runs were less than 5 MPa. A temperature gradient of ±3°C along 3 cm hot zone of the IHPV was controlled and monitored by four S-type (Pt–$Pt_{90}Rh_{10}$) thermocouples. The run duration varied between 15 and 95 hours (Table 1), except for one 3 hours run. The samples were quenched at rate of about 150°C/sec using a rapid-quench technique described by Berndt et al. (2002).

The redox conditions in the experiments were controlled by using an Ar or Ar-H_2 gas mixture in the IHPV and by addition of various proportions of H_2O and CO_2 to the capsules to vary the water activity (aH_2O). Permeation of H_2 through the capsule walls and reaction of H_2 with water according to the water dissociation reaction $H_2 + 1/2O_2 = H_2O$ controlled the fugacity of oxygen in the capsules, which can be calculated for every run using the equation $\log fO_2^{capsule} = \log fO_2^{IHPV} + 2\log(aH_2O)$ (see also Botcharnikov et al., 2005). According to the determination of Schuessler et al. (2008), the intrinsic redox conditions of the used IHPV ($\log fO_2^{IHPV}$), i.e., conditions of pure Ar gas pressure medium, are about QFM+3.3 (i.e., fO_2 is 3.3 log units higher than that of the QFM buffer) at aH_2O=1. The water activity in every capsule from water-undersaturated series was determined from the concentration of H_2O in the glass according to the model of Burnham (1975, 1979). One water-undersaturated experiment was performed with an Ar-H_2 gas mixture adjusted to achieve fO_2 of QFM-0.5. The estimated redox conditions in the entire dataset varied in a range of ΔQFM= -0.5 to +3.2 (Table 1).

2.3 ANALYTICAL METHODS

2.3.1. Electron microprobe

Major element concentrations in glass and mineral phases of experimental products, glasses of non-heated natural melt inclusions were determined with electron microprobe Cameca SX100 (Institut für Mineralogie, Leibniz Universität Hannover, Germany). Mineral phases were analyzed with a focused electron beam using 15 keV accelerating voltage and 15 nA beam current. Glasses were analyzed with a defocused beam (5 to 20 μm in diameter), 15 keV accelerating voltage and 4 nA beam current. Two samples from the V-series (V13 and V18) contained quench phases (amphibole) in the matrix glass. In order to include these quench phases into analysis of the glass, areas with a homogeneous distribution of small amphiboles were selected, the spot size was increased to 50 μm and the beam current was set up to 30 or 60 nA (both conditions provided the same glass composition for an individual sample). Sodium and K were analyzed first to minimize the alkali loss. Aluminum, Ca, Mn and Ni in olivines from the V-series were analyzed using 100 nA beam current and 30 s accumulation time. Each phase in the experimental products was analyzed 3 to 10 times. Glass inclusions were analyzed at 2-3 points. Calibration of the analyses was performed using a number of mineral and glass standards (wollastonite for Si and Ca, orthoclase for K, albite for Na, Al_2O_3, MgO, Fe_2O_3, Mn_3O_4, TiO_2, Cr_2O_3, apatite for P. The glass compositions were corrected against reference basaltic glass VG-2 (USNM 111240/52) from the Smithsonian Institute, USA (Jarosewich et al., 1980).

Glasses of three re-heated melt inclusions and host olivines for all inclusions were analyzed employing a JEOL JXA 8200 at GEOMAR (Kiel, Germany). Major elements in glasses were analyzed at 15kV, 6 nA and a beam defocused to 5 μm. Microprobe reference materials of the Smithsonian Institute (Jarosewich et al., 1980) were used for calibration (basaltic glass VG-A99, rhyolitic glass VG568, scapolite R6600-1) and for monitoring the data quality. Olivines

were analyzed with a focused beam at 100 nA and 15 kV. The San Carlos olivine (Jarosewich et al., 1980; Sobolev et al., 2007) was used as a reference. Details of the analytical technique can be found in Mironov et al. (2015) and Ponomareva et al. (2017).

2.3.2 Laser ablation inductively-coupled plasma mass spectrometry (LA-ICP-MS)

Concentrations of vanadium in glasses and olivines from experimental products of "V" series were determined by Laser Ablation (LA) ICP-MS at the Leibniz Universität Hannover. The LA-ICP-MS system is composed of an Element XR™ (Thermo Scientific™) fast scanning sector field inductively coupled plasma mass spectrometer in combination with an in-house modified laser ablation system which is based on a Spectra-Physics™ femtosecond (Ti:Sapphire) laser (Solstice™ system) operating in the deep UV at 194 nm (e.g., Albrecht et al., 2014). An Ar-He gas mixture was used for aerosol transport from the ablation cell and as a plasma-forming medium. The ablation of experimental glasses and reference material (NIST610) was conducted at 10 Hz and with a spot size of about 40 µm in diameter. Small olivine grains were analyzed using 5-15 µm beam size. The oxide production rate was kept at ThO^+/Th^+<0.35%at maximum sensitivity. The concentration of Si in olivines and glasses, analyzed by EMPA, was used as an internal reference material, and ^{29}Si was analyzed by LA-ICP-MS. Data reduction employed the LAMTRACE software (Jackson, 2008).

Experimental products from "N" series as well as natural melt inclusions and host olivines were analyzed with LA-ICP-MS using Agilent 7500s quadrupole mass-spectrometer coupled with the 193 nm Excimer Laser-Ablation system GeoLasTM Pro (Coherent™) at the Institute of Geosciences of the Christian-Albrechts University of Kiel using standards and instrumental conditions as described by Sobolev et al. (2016). For every experimental run, 2 - 3 glass areas were analyzed with 24 µm laser spot and 8-10 olivine grains with 10-16 µm laser spot. Natural glass inclusions were analyzed in 1 - 2 spots of 24 µm, the host olivines in 2 spots at about half

melt inclusion diameter distances from the olivine-glass boundary with laser spot of 24 µm. The obtained time-resolved spectra were evaluated using the Glitter™ Software (Griffin et al., 2008) to define integration window, avoiding contamination of olivine by glass or mineral inclusions as much as possible, and to calculate concentration values, their precision (in run 1σ) and detection limits. Measured intensities were normalized to ^{29}Si (olivine) and ^{43}Ca (glass) and converted to weight concentration values by matching the sum of Si, Al, Fe, Mn, Mg, Ni and Ca oxides to 100% wt% for olivine and by using CaO concentrations measured by electron probe for internal standardization for glass. Correction of Sc concentrations in olivine for interference with $^{29}Si^{16}O^{+}$ was performed using $^{29}Si^{16}O^{+}/^{29}Si^{+}$ measured on Sc-free synthetic silica and the intensity of $^{29}Si^{+}$ signal in olivine. The detection limit for vanadium was estimated to vary from 0.02 ppm at a laser spot diameter of 24 µm to 0.1 ppm at laser spot diameter 10 µm. The calibration was performed using the set of microanalytical reference materials (glasses) SRM NIST612, GOR128-G, KL2-G and BCR-2G (Jochum et al., 2006; 2011; Wilson, 1997) and an in-house reference sample of pressed nanoparticulate powder pellet made of olivine from the San Carlos mine and analyzed by solution ICP-MS (Garbe-Schönberg and Müller, 2014). The majority of the data were obtained in 2015 and verified in 2016 using the new olivine reference material MongOL Sh11-2 (Batanova et al., 2017). Before measurements, the instrument was tuned using the SRM NIST-612 glass to get maximum sensitivity at minimum oxide production rate (with $ThO^{+}/Th^{+}<0.3$).

A comparison of results obtained in the two ICP-MS labs revealed no considerable systematic discrepancy (i.e., within 10%) of the measured V concentrations in olivine and glass from two “V”-series samples (Table 1).

Olivine crystals produced in water-saturated “V” series were large enough (>50 µm) for unproblematic high quality analysis (Fig. 2 A, B). Aluminium concentrations are particularly sensitive to contamination of olivine analyses by glass, plagioclase or spinel. Low Al

concentrations in "V"-series olivine and good agreement between EMPA and LA-ICP-MS measurements (Appendix A1) confirm that these data are not affected by entrapment of other phases present in experimental charges. Replicate analyses on the same olivine grain for samples V8 (2 spots), V13 (3 spots) and V18 (2 spots) showed variations in V concentrations within analytical uncertainty for several olivine grains from individual sample.

Olivine in the water-undersaturated "N"-series had typically smaller size (< 30 μm) and associated with other crystal phases. These phases (plagioclase, Ti-magnetite) together with glass were also present as inclusions in olivine (Fig. 2 C-E). Glass and Ti-magnetite contained vanadium in amounts which exceed significantly those in olivine. Hence, if these phases were trapped during laser ablation of olivine, V concentrations in olivine were overestimated. To avoid or minimize this contamination effect, V (and other trace elements) concentrations in olivines were always calculated for the part of time-resolved spectra with the lowest Al/Si (Fig. 3A). The V data (and other trace elements) were then examined for contamination by plotting the data against the Al content determined for the same LA-ICP-MS spot. In three runs we observed no correlation of V and Al contents (# N5, 34, 86), indicating contamination by micro inclusions of plagioclase containing very low V concentrations. In the other runs, we found near-linear correlations between concentrations of Al and V for olivine data (runs # 33, 45, 60, 69), which were interpreted as evidence for contamination of olivine by small and variable amounts of glass or by mixture of glass and plagioclase in relatively constant proportions. Strongly contaminated points (>1 wt% Al) or those significantly deviating from the correlations were excluded as they were likely disproportionally contaminated by plagioclase and/or Ti-magnetite (Fig. 3B). The corrected V concentrations in olivine were then calculated from a linear regression between measured V and Al concentrations, assuming that Al in olivine was 100 ppm (Fig. 3B). Based on the Al content in large experimental olivine crystals, which did not contain plagioclase inclusions, the uncertainty of this Al concentration is ±50 ppm (Fig. 3A, B;

Table 1). This uncertainty in Al content has negligible effect on the corrected V values (Fig. 3B). In all cases, extrapolated V contents in olivine were close to minimal measured concentrations in every run (e.g., run N45 in Fig. 3B) or somewhat lower. Concentrations of all other trace elements in olivine of "N"-series were checked for contamination and corrected in a similar way as described for vanadium.

Uncertainties for V are 2 SE (standard error of mean, 95% confidence level) were calculated as 2*1s/SQRT(n), where 1s is standard deviation and n is the number of analyzes. Uncertainty of D_V was calculated using a conventional rule for error propagation: Error(X/Y) = $X/Y*[(ErrorX/X)^2+(ErrorY/Y)^2)]^{0.5}$.

2.3.3 SIMS

Secondary ion mass-spectrometry (SIMS) was used to estimate the concentrations of water in melt inclusions. Analyses were performed with a CAMECA ims4f at the Yaroslavl' Branch of the Institute of Physics and Technology (a former Institute for Microelectronics, Yaroslavl', Russia), following the procedure described by Portnyagin et al. (2007). Accuracy and precision of the analyses are estimated to be better than 15%. The background signal for $^1H^+$ converted to weight percent of water equivalent was 0.01–0.02 wt.% as measured on nominally anhydrous olivine phenocrysts from highly depleted MORB from the Siqueiros Fracture Zone (Sobolev and Chaussidon, 1996).

2.3.4 FTIR

Fourier-transform infrared spectroscopy (FTIR) was applied for the determination of H_2O in glass in the run products of "N"-series with relatively low crystallinity where glass areas could be visually found in microscope and diameter of spot for the analysis was adjusted to the size of glass area. Both mid-infrared (MIR) and near-infrared (NIR) ranges were used for

measurements depending on H_2O-concentration in glasses. The method is described in details by Shishkina et al. (2010, 2014). Molar absorption coefficients for basaltic glasses determined by Shishkina et al. (2010) were used for calculations: 60 g/(mol*l) for the 3550 cm^{-1} H_2O band, 0.79 g/(mol*l) for the 4500 cm^{-1} band (hydroxyl group) and the 5200 cm^{-1} band (molecular water). The H_2O concentrations in experimental glasses determined by FTIR were used for the estimation of aH_2O and fO_2 in every experimental run (capsule).

The water contents in the water-saturated experiments of the "V"-series have not been directly measured. We assumed the H_2O in glasses of these runs to be close to the H_2O solubility in the Mutnovsky basalt at 300 MPa (6.25 wt.% H_2O; Shishkina et al., 2010). The water contents estimated from the EMPA analyses by difference to the analytical total is 6-8 wt%, and that is close to the expected values (Table 1).

2.4 MELT INCLUSIONS

Melt inclusions in olivine phenocrysts were studied in samples of basaltic tephra (KM9-10 and KM9-11), and lava (N71, N72) (Fig. 2-F, Table 2, Appendix-A2). The detailed petrological and geochemical information for these samples is provided by Shishkina (2012) and Duggen et al. (2007). Large ~1 mm sized olivine phenocrysts have been separated from the rock samples and investigated under an optical microscope to locate melt inclusions. Melt inclusions in olivine from slowly cooled lava samples (N71 and N72) were found to be partially crystallized. Prior to analyses, they were reheated with the aim to eliminate the effects of post entrapment crystallization inside the inclusions. Re-heating experiments were performed in the "Vernadsky"-type high-temperature micro-heating stage (e.g., Danyushevsky et al., 2002) with optical control at the Vernadsky Institute (Moscow, Russia). Single olivine grains containing melt inclusions were heated in the furnace up to the temperature at which daughter crystals were completely molten. The duration of the re-heating experiments was typically 5 to 10

minutes. At the end of the experiment, the inclusions were quenched by switching off the electric supply. Detailed description of the technique can be found in Portnyagin et al. (2007). Melt inclusions in olivine from rapidly quenched tephra samples (samples KM9-10 and KM9-11) were glassy (contained no daughter phases except for a fluid bubble) and required no experimental homogenization before analysis. Prior to analysis, natural glassy and reheated inclusions were exposed by gradual polishing off the host olivine.

To eliminate effects of olivine crystallization or melting on the composition of melt inclusions, their compositions were re-calculated to be in equilibrium with their host olivine using the Petrolog3 software (Danyushevsky and Plechov, 2011). Naturally quenched (glassy) inclusions were recalculated using the option „Reverse crystallization“, which simulates the addition of small amounts of equilibrium olivine to the melt until achievement of equilibrium with the host olivine. The model of Ford et al. (1983) was applied to calculate olivine-melt equilibria. Calculations were performed for a pressure of 100 MPa and redox conditions of QFM+2. The Fe^{+2}/Fe^{+3} ratio in the melt was calculated using the model of Borisov and Shapkin (1990). Re-heated melt inclusions were re-calculated to be in equilibrium with the host olivine using the “Fe-loss” (or “Fe-gain”) option. In this case, the reconstruction of melt inclusion compositions was performed assuming that the initial Fe total content in melt is equal to that in the host rock (about 9.4 wt.% FeO for samples N71 and N72). Other parameters for calculation were the same as for glassy inclusions. All calculations were performed assuming H_2O-free melt composition. The effect of H_2O on the liquidus temperature of the initially trapped melts was estimated using the model of Almeev et al. (2007) and the H_2O content measured by SIMS. For melt inclusions from lavas, their initial H_2O content was assumed to be 2 wt.% as these inclusions lost nearly all their initial water due to slow cooling after eruption (e.g. Portnyagin et al., 2008). The calculated melt inclusion compositions and liquidus temperatures are listed in Table 2.

Concentrations of V, Y and Sc in initially trapped melts (C_i^o) were then calculated using the mass-balance equation $C_i^o = C_i (1-X_{Ol}) + C_i^{Ol} X_{Ol}$, where C_i and C_i^{Ol} are LA-ICP-MS data for glass and olivine, respectively, and X_{Ol} is the fraction of olivine that crystallized or melted as determined in the Petrolog3 calculations. The measured compositions of melt inclusions are presented in Appendix A-2, and their reconstructed initial compositions and host olivine compositions in Table 2.

3. RESULTS

3.1 EXPERIMENTAL PRODUCTS

The experiments were conducted at pressures and temperatures that are thought to be close to the conditions prevailing in a magma chamber below Mutnovsky volcano (Shishkina et al., 2010; 2012; this study). Eleven runs were performed at 0.3 GPa in a temperature range of 1025 to 1150°C, and the fO_2 values range between QFM-0.5 to QFM +3.2. One experiment was additionally performed at 0.1 GPa, 1075°C and QFM+3.2. All samples contained euhedral to subhedral olivine crystals (Fo 80.2 – 84.9) which were large enough (up to 150 μm in "V"-series and up to 30 μm in "N"-series) to be analyzed by LA-ICP-MS (Table 1, Fig.2). The water-undersaturated run products of "N"-series contained olivine crystals often with tiny poikillitic inclusions of plagioclase, sometimes magnetite and glass (Fig. 2 C-E). Plagioclase was also present as individual elongated crystals up to 10 μm in the glass matrix. Some experiments contained crystals of clinopyroxene with sizes up to 15 μm in "N"-series (N72-33, -34 and -69) and up to 70 μm in "V"-series (V25 and V26) (Table 1, Fig. 2D and 2B, respectively). Two water-saturated samples (V13 and V18) were not properly quenched and contain quench amphibole crystals in the matrix glass.

Major elements and V concentrations in experimental glasses and olivines are presented in Table 1. The complete set of analytical data can be found in a supplementary table (Appendix-

A-1). Within analytical precision, mineral and glass phases in every run have homogeneous compositions which is an indication for the attainment of chemical equilibrium. Redox equilibrium in high-T hydrous basaltic systems run in AuPd or even Au capsules can be achieved in minutes to a few hours (Berndt et al., 2002). Since we did not observe a detectable zonation in olivines (indicative also of redox disequilibrium, Berndt et al., 2002), we assume complete equilibration of the systems in the course of the experiments. The values of $Kd_{Fe2+-Mg}^{Ol-Melt}$ calculated using FeO and MgO contents in olivines and glasses from the run products with Fe^{2+} estimated by the model of Kress and Carmichael (1991) vary mostly between 0.32 - 0.36, which are typical for the equilibrium olivine-melt compositions (e.g., Toplis, 2005) (Table 1). Slightly elevated Kd's (0.38-0.39) in two runs performed at oxidizing conditions can be attributed to somewhat overestimated fO_2 in these runs.

3.2 VANADIUM CONCENTRATIONS AND PARTITIONING BETWEEN OLIVINE AND MELT

The concentration of vanadium varies between 2.3 and 26.6 ppm V in experimental olivines and between 263 and 431 ppm in experimental glasses. These values are very close to the vanadium concentrations in natural Mutnovsky melt inclusions and host olivines (Fig. 4A, Table 2), hence indicating that our experiments reproduced closely the natural conditions of Mutnovsky magma crystallization.

The partition coefficient D_V^{Ol-M} for Mutnovsky basalt varies between 0.008 and 0.081 (corresponding to $\log D_V^{Ol-M}$ between -2.11 and -1.09) and shows a strong negative correlation with ΔQFM (Fig. 4 B), which is generally consistent with previously published experimental results. This correlation for 12 experiments employing the Mutnovsky basalt can be fitted by linear regressions:

$$\log D_V^{Ol-M} = -0.285^{+0.025}_{-0.045} \Delta\,\mathrm{QFM} - 1.150^{+0.023}_{-0.060} \quad (1)$$

$$\Delta\,\mathrm{QFM} = -3.26^{+0.47}_{-0.52} \log D_V^{Ol-M} - 3.73^{+0.75}_{-0.85} \quad (2)$$

where ΔQFM is the difference between determined logfO_2, and logfO_2 being buffered by the Quartz-Fayalite-Magnetite buffer at a given T and P.

3.3 COMPOSITION OF MELT INCLUSIONS

Nine naturally quenched melt inclusions with sizes larger than 50 µm in olivine phenocrysts from Mutnovsky basaltic tephra (samples KM9-10, 11) and three re-homogenized melt inclusions from basaltic lavas (N71, N72) were analyzed for major-element, volatiles, V, Sc and Y concentrations (Fig. 2F, Table 2, Appendix A-2).

The compositions of the host-olivines are in the range of Fo 78.2 - 79.8 for glassy inclusions and Fo80.9 – 84.0 for the re-heated ones. According to the Petrolog3 calculations, glassy inclusions crystallized 1.1 - 6.2 % of olivine after entrapment, which had to be dissolved back into the melt to achieve the equilibrium compositions. Re-heated inclusions required either crystallization or melting of 2.5 to 4.8 % olivine to achieve equilibrium with their host. The temperatures of melt-olivine equilibrium estimated for melt inclusions are in the range of 1034 - 1106°C, in remarkable agreement with the temperatures of 1057 – 1129°C estimated using the Y/Sc thermometer (Mallmann and O`Neill, 2013).

The initially trapped inclusions have basaltic compositions with 46.7 to 53.4 wt.% SiO_2, 4.3 to 6.6 wt.% MgO and 266 to 451 ppm V, which overlap the range of Mutnovsky whole rock compositions (e.g., Duggen et al., 2007). Vanadium concentrations in host olivines vary between 4.2 and 6.6 ppm, which corresponds to a narrow range of $D_V^{Ol\text{-}M}$ values between 0.0142 and 0.0193 ($\log D_V^{Ol\text{-}M}$ between -1.72 and -1.85) (Fig. 4A). According to equation (2), the olivine-melt partitioning corresponds to ΔQFM = 1.8 -2.3 (Fig. 7).

3.4 OLIVINE - SPINEL EQUILIBRIA IN MUTNOVSKY ROCKS

In Mutnovsky basalts, spinel group minerals were usually found as inclusions in olivine phenocrysts with Fo-numbers between 77 and 84. Spinel compositions have variable Fe, Mg, Al, Cr and Ti contents and vary along the Fe-Ti and Cr-Al trends (Barnes and Roeder, 2001) from Ti-magnetite to low-Cr, high-Al spinel (hercynite-pleonaste; Cr/(Cr+Al) < 0.3) (Deer et al., 1992; Appendix A-3).

Ballhaus et al. (1991) proposed a widely used oxybarometer based on the olivine-spinel equilibrium. This oxybarometer was calibrated using a series of experiments with olivine (Fo>85), spinel and orthopyroxene on the liquidus, which were conducted at various pressures, temperatures and aH_2O conditions. The compositions of olivine and spinel in Mutnovsky rocks are outside of the calibrated compositional range given by Ballhaus et al. (1991). Keeping this limitation in mind, the model was applied to estimate fO_2 and equilibrium temperature for 34 pairs of the most Mg-rich olivine (Fo80.6–83.7) and spinel with $Fe^{3+}/(Fe^{3+}+Al+Cr)<0.20$ and Al/(Al+Cr+Fe3+)>0.5 (Appendix A-3). The fO_2 estimates were corrected by 0.2 logfO_2 units to account for the absence of orthopyroxene from the liquidus assemblage (Ballhaus et al., 1991). Assuming a crystallization pressure of 0.1 GPa for these olivine-spinel pairs, the temperature and oxygen fugacity were estimated to range from 890 to 1034°C and from QFM+1.7 to QFM+2.1, respectively. (Appendix A-3, Fig. 7).

Recently, a new model of the olivine-spinel oxybarometer based on a larger experimental dataset was presented by Nikolaev et al. (2016). This model is applicable to orthopyroxene-free systems and was calibrated for a much wider range of spinel and olivine compositions compared to the model by Ballhaus et al. (1991). The application of the model to the same set of Mutnovsky olivine-spinel pairs gives redox conditions between QFM+0.6 and QFM+1.5, which is about one log unit fO_2 below the results obtained using the model of Ballhaus et al. (1991) (Appendix A-3, Fig. 7). Apparently, the discrepancy between the results exceeds significantly the reported accuracy (ca. 0.25 fO_2 log units) of both oxybarometers.

4. DISCUSSION

4.1. COMPARISON WITH OTHER EXPERIMENTAL DATASETS

In all previously published experimental studies of V partitioning, the starting mixtures were doped with different amounts of vanadium (in form of V_2O_3 or V_2O_5), with up to 1.7 wt.% of V_2O_3 (Canil, 1997; 1999; Canil and Fedortchouk, 2001), which resulted in much higher (10-10000 times) concentrations of V in experimental olivines and glasses in comparison to our experiments and concentrations in natural rocks (Fig. 4A). The values for $D_V^{Ol\text{-}M}$ obtained in this study are nevertheless comparable to those obtained in doped experiments at a given ΔQFM (Fig. 4B). The results extending the experimental database to the range of natural concentrations confirm that V doping does not significantly affect the experimental data on V partitioning, and that V still obeys Henry's law at higher concentrations. This reaffirms the validity of previously reported results in application to natural magmas and opens the possibility for direct comparison of data from our and previous studies and analysis of the possible reasons for $D_V^{Ol\text{-}M}$ variability.

The negative correlation of $D_V^{Ol\text{-}M}$ and ΔQFM obtained in our experiments on Mutnovsky basalt is in good agreement with previously published data (e.g., Canil, 1997; Canil and Fedortchouk, 2001; Mallmann and O`Neill, 2013; Fig. 4B). The slope of the correlation is steeper compared to data of Canil (1997). Furthermore, $D_V^{Ol\text{-}M}$ values obtained in this study are close to the maximum values reported in previous experimental studies at a given ΔQFM (Fig. 4B).

The majority of previous studies revealed no detectable effects of pressure, temperature, olivine or melt composition on $D_V^{Ol\text{-}M}$ (e.g., Canil, 1997; Canil and Fedortchouk, 2001; Shearer et al., 2006; Papike et al., 2013; Laubier et al., 2014). However, the compilation of literature data shows that variations of $D_V^{Ol\text{-}M}$ at given redox conditions reach up to one order of magnitude and indicates that some factors other than fO_2 should be taken into account to precisely

describe V partitioning for a wide range of possible conditions (Figs. 1 A-B, 5A). A recent parameterization by Mallmann and O`Neill (2013) attempted to take into account the possible dependence of $D_V^{Ol-M}$ on $fO_2$, T and olivine and melt composition. Although our data are not correctly predicted by the model of Mallmann and O`Neill (2013) within the reported uncertainty (Fig. 5B), this model does predict a relatively high D_V^{Ol-M} for the experimental conditions of this study and thus confirms that some additional parameters should be taken into account for an accurate description of D_V^{Ol-M}.

Our experimental data were obtained at relatively low pressures, for low alkali tholeiitic composition and moderately magnesian olivine. Thus, the investigated pressure and compositional parameters are similar to the majority of other data obtained for MORB-like compositions (e.g., Hawaiian tholeiitic basalt; Canil and Fedortchouk, 2001); MORB and basaltic andesite (Laubier et al., 2014); and MORB with addition of olivine (Mallmann and O`Neill, 2013). Our experiments were, however, performed at much lower temperatures (T< 1150°C) compared to most published data (Fig. 1C). It is thus plausible that the tendency toward higher D_V^{Ol-M} at given ΔQFM observed in our data may be related to the low equilibration temperature. An inverse dependence of D_V^{Ol-M} on temperature is also proposed in the model of Mallmann and O`Neill (2013) (Fig. 5A).

Our experiments were performed at various H_2O activity, in contrast to all previously published vanadium partitioning experiments carried at anhydrous conditions. However, no detectable effect of H_2O on olivine-melt V partitioning was detected, as clearly indicated by the narrow range of D_V^{Ol-M} obtained at fO_2 near QFM and for H_2O content of the melt ranging from 0.4 to 6.3 wt%.

4.2 CALIBRATION OF OXYBAROMETER FOR LOW TEMPERATURE MAGMAS

In order to verify the hypothesis of significant temperature dependence of D_V^{Ol-M}, we

compared our data with results obtained previously at temperatures below and above 1250°C. Previously published results obtained for natural compositions at T <1250°C include MORB and basaltic andesite (Laubier et al., 2014), some komatiites (Canil, 1997), Hawaiian tholeiite (Canil and Fedortchouk, 2001), MORB (Mallmann and O`Neill, 2013), and Martian basalt (Papike et al., 2013) (Fig. 5B; Appendix, A-4). Data reported for Na-rich starting compositions (Na_2O >6 wt.%) were excluded from comparison as they show significantly lower $D_V^{Ol\text{-}M}$ and likely testify a compositional effect of Na_2O on V partitioning (Fig. 5B). As illustrated in Fig. 5, the data obtained in our experiments agree very well with the previously published low-T data. In contrast, the experiments performed at T >1250°C show systematically lower $D_V^{Ol\text{-}M}$ at a given ΔQFM.

Figure 6 shows how the different models reproduce the oxygen fugacity of experimental data at temperatures below 1250°C. The model proposed by Mallmann and O'Neill (2013) reproduces experimental ΔQFM well for relatively reduced conditions (ΔQFM<0) and tends to overestimate ΔQFM at more oxidized conditions. The model of Canil and Fedortchouk (2001) underestimates ΔQFM at reduced conditions and shows a good agreement with experimental data for oxidizing conditions. The observed discrepancy between the low-T data and the predictions from the most popular V-in-olivine oxybarometers implies that the barometers should be refined to better describe the dependence of $D_V^{Ol\text{-}M}$ on fO_2 at low temperature. This can be done using new data from this study and recent works by Papike et al. (2013) and Laubier et al. (2014), which were not included in previously published calibrations.

For the recalibration of V oxybarometer for low temperature basaltic magmas, we used 12 experiments from this study together with 47 experiments performed at T ≤1250°C in the fO_2 range of -2.0 < ΔQFM < 3.2 with melts containing less than 12 wt% MgO and less than 4 wt.% Na_2O, selected from previously published data (Canil, 1997: 3 runs with starting komatiite composition; Canil and Fedortchouk, 2001: 1 run with Hawaiian tholeiite; Mallmann and

O`Neill, 2013: 17 runs with MORB; Papike et al., 2013: 2 runs with Martian basalt; Laubier et al., 2014: 12 runs with MORB and 12 runs with basaltic andesite) (Appendix A-4).

The correlation between $D_V^{Ol\text{-}M}$ and ΔQFM for such magmas can be described by following linear equations (see Fig. 5B):

$$\log D_V^{Ol-M} = -0.275^{+0.026}_{-0.025}\Delta\text{QFM} - 1.077^{+0.016}_{-0.040} \quad (3)$$

$$\Delta\text{QFM} = -3.07^{+0.26}_{-0.29}\log D_V^{Ol-M} - 3.34^{+0.40}_{-0.49} \quad (4)$$

The standard error (2SE, 95%) for ΔQFM values calculated with the equation 4 may be estimated as:

$$2\text{SE}\ (\Delta\text{QFM}) = -0.275\log D_V^{Ol-M} + 0.4 \quad (5).$$

The new calibration of the V-in-olivine oxybarometer was applied to estimate the redox conditions of Mutnovsky magmas using V concentrations in melt inclusions and host olivine from basaltic tephra and lavas of Mutnovsky volcano. The ΔQFM values determined using the more general equation (4) vary between +1.9 to +2.3 (Table 2). Redox conditions obtained using the equation of Canil (2001) are similar within 0.1 logfO_2 values (Fig. 7; Table 2). The ΔQFM values estimated with the model of Mallmann and O'Neill (2013) are in the range of +2.6 to +3.2 which is 0.7 to 1.1 logfO_2 units higher compared to our estimates (Fig. 7, Table 2). The ΔQFM values estimated from equations (2) or (4) for Mutnovsky melts are very close to the redox conditions determined from the compositions of coexisting spinel and olivine using the model of Ballhaus et al. (1991). The calculations using the model of Nikolaev et al. (2016) suggest significantly more reduced conditions compared to other methods (Fig.7, Appendix A-3).

In summary, equation (4) and the models of Canil and Fedortchouk (2001) and Ballhaus et al. (1991) yield the most consistent estimates of ΔQFM for the range of compositions and P-T

conditions corresponding to moderately evolved Mutnovsky magmas.

4.3 USING MELT INCLUSIONS IN OLIVINE FOR OXYBAROMETRY

Our new as well as recently published experimental data allowed refining the V-in-olivine oxybarometer for the low temperature conditions, which are particularly relevant to the origin and evolution of magmas in subduction related settings. Using melt inclusions in olivine may be very promising as it can provide information on redox conditions at a specific stage of magma evolution (i.e., when the melt inclusion in olivine is formed). One important issue must be, however, considered before application of the V-in-olivine oxybarometry to natural samples. This issue concerns potential post-entrapment modification of melt inclusions in olivine. If the concentration of vanadium in a melt inclusion or in a host olivine is affected by such a modification, the results of oxybarometry will be erroneous.

Initial $D_V^{Ol\text{-}M}$ values can be affected by post-entrapment crystallization or melting of olivine on the walls of the melt inclusion, hence resulting in an increase or decrease of the initial V concentrations in melt. The effect of these processes can be accounted for by using mass balance calculations. For example, crystallization of 10 wt% olivine from the inclusion will result in an overestimation of the fO_2 by about 0.15 log units, which is a relatively small error in comparison with the estimated accuracy of V-in-olivine oxybarometers from this and previously published studies (e.g., ±0.3 log units for equation 4). As vanadium is a highly incompatible element in olivine, the reconstruction of the initial composition for natural melt inclusions by modeling of reverse crystallization is not problematic but still recommended to improve the precision of the oxybarometry based on V partitioning.

Newcombe et al. (2014) described significant effects of diffusion-driven inter-element fractionation inside slowly cooled melt inclusions, which cannot be reversed by simple modeling of olivine addition and thus are potentially capable to affect results of V-in-olivine

oxybarometry. In order to estimate the magnitude of this effect, we used data for one arbitrary chosen melt inclusion (Siq7) from the supplementary tables provided by Newcombe et al (2014) and calculated the compositions of melts in equilibrium with the host olivine Fo89.4 for every microprobe analysis made across this inclusion with diameter of 100 μm. The largest difference of up to 15 rel.% between maximum and minimum values in the estimated "initial" melts was found for Al. Assuming that spatial resolution of LA-ICP-MS analyses is as good as for microprobe (ca. 2 μm), and the V diffusivity is identical to that of Al, the intra-inclusion variations can introduce an uncertainty of ca. 0.2 log units in the estimated ΔQFM. If we apply a more commonly used spot size of 20-30 μm, the maximum difference in the Al content between "initial" melts reconstructed from analyses in four spots made across this inclusion will not exceed 5 rel.%, which is a typical precision of LA-ICP-MS data. Taking titanium as more probable analog of V in moderately oxidized melts reveals no significant effect of intra-inclusion fractionation, which apparently did not exceed the analytical uncertainty of 8 rel.% (2RSD for 50 data points) for Ti in the inclusion tested.

Judging from these results, we expect a relatively minor to negligible effect of intra-inclusion element fractionation on the results of V-in-olivine oxybarometry. The effects can be further minimized by reconstruction of initial melt inclusion compositions taking into account possible Fe-loss (Danyushevsky at al., 2002). In order to avoid a biased effect of just one reference element, usually Ca, which is unfortunately the most strongly fractionated element in melt inclusions studied by Newcombe et al. (2014), on quantification LA-ICP-MS data, normalization of oxides to 100% for quantification of LA-ICP-MS data appears to be a more robust approach (e.g., Pettke et al., 2004). Finally, it is certainly possible to quantify the composition of the entire, slightly exposed or unexposed on surface, inclusions (Pettke et al., 2004), which may eliminate completely all effects of intra-inclusion heterogeneity as well as some short-distance effects of inclusion re-equilibration with olivine. This approach will,

however, leave no material for next analyses and produce less precise data for low abundance elements due to strong dilution of analytical signal by olivine component.

A more serious problem may be the diffusive re-equilibration of melt inclusions with olivine due to changing external conditions, thus affecting the V partitioning (e.g., magma cooling or oxidation). To estimate the time scales on which V diffusion in olivine affects the composition of melt inclusions, we applied a model of Qin et al. (1992) and published data on V diffusivity in olivine (Spandler et al., 2010) and $D_V^{Ol\text{-}M}$ data. Figure 8 illustrates the time necessary for re-equilibration of a melt inclusion with a diameter of 50 µm located in the center of a 1 mm-sized olivine crystal at QFM and QFM+2, respectively, and at 1300°C. The modelling shows that 50% re-equilibration of the inclusion will be achieved within about 1.5 years at QFM and in about 2 years at QFM+2. The re-equilibration time will shorten by decreasing the size of the melt inclusion and/or olivine and become longer with decreasing temperature, as the diffusion rate slows down exponentially at decreasing temperature. Unfortunately, no data on V diffusivity is available at temperatures lower than 1300°C. The calculated residence times should, therefore, be considered as very conservative estimates for the survival time of a melt inclusion in low temperature island-arc magmas with respect to the vanadium partitioning. Real re-equilibration times may be 1-2 orders of magnitude longer at 1100-1200^{o}C.

Though the re-equilibration times can be estimated to be relatively short on the geological time-scale, they are at least 2 orders of magnitude longer compared to a few hours to few days required to re-equilibrate melt inclusions with respect to H_2O or fO_2 (Portnyagin et al., 2008; Gaetani et al., 2012; Bucholz et al., 2013). This means that the V-in-olivine oxybarometer may be much more resistant to possible changes of external fO_2 conditions in comparison with oxybarometric methods based on the direct determination of Fe^{2+}/Fe^{3+} and S^{2-}/S^{6+} in melt inclusions.

Finally we emphasize that the analysis of the true host olivine is a prerequisite for correct

application of the V-in-olivine oxybarometer. This may be problematic for some pseudo-primary melt inclusions formed by entrapment of melt into voids formed by partial dissolution of olivine at some stage of its magmatic history. A nice example of olivine with a complex history preserved in phosphorus zoning was recently published by Manzini et al. (2017) and this example illustrates that a careful examination of the host olivine is necessary.

Implications

The study presents new experimental data on vanadium partitioning between olivine and melt for high-Al island arc tholeiitic basalt of Mutnovsky volcano conducted at logfO_2 in the range of ΔQFM = -0.5 to +3.2, temperature range of 1025-1150°C and pressures of 0.1 and 0.3 GPa. The new experiments and recently published data allowed us to refine the V-in-olivine oxybarometer for relatively low temperature conditions (<1250°C) that are relevant for typical island-arc magmas.

As an example of application of the refined oxybarometer, we estimate fO_2 for Mutnovsky basalts by using data on V partitioning between olivine and melt inclusions from basaltic tephra and lavas. The redox conditions were estimated to be QFM+1.9 to +2.3, indicating strongly oxidized conditions, but not as much as predicted by some previously published models. Due to the relatively slow diffusivity of vanadium in olivine, the V-in-olivine oxybarometer may be more appropriate to track changing fO_2 conditions in magmatic systems, in particular for primitive melts, than direct estimates of Fe^{2+}/Fe^{3+} or S^{2-}/S^{6+} in melt inclusions.

Acknowledgements

This research has been supported by the Russian Science Foundation (grant 14-17- 000582) and by the German Science Foundation (DFG projects Ho1337/21, Ho1337/19 and Bo2941/3-1). We thank C. Godeck for the help with performing the experiments, U. Westernströer for help with

the LA-ICP-MS at CAU Kiel, I. Horn for help with the LA-ICP-MS at LU Hannover. Also we thank M. Brounce and an anonymous reviewer whose critical comments helped to improve the original manuscript. The editorial work of S. Straub is greatly appreciated.

LITERATURE

1) Albrecht, M., Derrey, I.T., Horn, I. Schuth, S., and Weyer, S. (2014) Quantification of trace element contents in frozen fluid inclusions by UV-fs-LA-ICP-MS analysis. Journal of Analytical Atomic Spectrometry, 29, 1034-1041.

2) Almeev, R.R., Holtz, F., Koepke, J., Parat, P., and Botcharnikov, R.E. (2007) The effect of H_2O on olivine crystallization in MORB: experimental calibration at 200 MPa. American Mineralogist, 92, 670–674.

3) Ballhaus, C.G., Berry, R.F., and Green, D.H. (1991) High pressure experimental calibration of the olivine-orthopyroxene-spinel oxygen geobarometer: implications for the oxidation state of the upper mantle. Contributions to Mineralogy and Petrology, 107, 27-40.

4) Barnes, S.J., Roeder, P.L. (2001) The range of spinel compositions in terrestrial mafic and ultramafic rocks. Journal of Petrology, 12, 2279-2302.

5) Batanova V, Sobolev A, Thompson J, Danyushevsky L, Goemann K, Portnyagin M, Garbe-Schoenberg D, Hauri E, Kimura J-I, Chang Q, Senda R, Chauvel C, Campillo S, Ionov D (2017) Preliminary Data on New Olivine Reference Material MongOL Sh11-2 for in situ Microanalysis. Goldschmidt2017 Abstract

6) Berndt, J., Liebske, C., Holtz, F., Freise, M., Nowak, M., Ziegenbein, D., Hurkuck, W., and Koepke, J. (2002) A combined rapid-quench and H2-membrane setup for internally heated pressure vessels: Description and application for water solubility in basaltic melts. American Mineralogist, 87, 1717–1726.

7) Borisov, A.A., and Shapkin, A.I. (1990) A new empirical equation rating Fe3+/Fe2+ in magmas to their composition, oxygen fugacity, and temperature. Geochemistry International, 27, 111-116. (translated from Geokhimiya, 6, 892-897, 1989).

8) Borisov, A.A., Kadik, A.A., Zharkova, Y.V., and Kalinichenko, N.V. (1987) Effects of oxygen fugacity on the ratio between valency forms of vanadium in magmas. Geochemistry International, 24, 15-20. (translated from Geokhimiya, 7, 915-920, 1986).

9) Botcharnikov, R.E., Koepke, J., Holtz, F., McCammon, C., Wilke, M. (2005) The effect of water activity on the oxidation and structural state of Fe in a ferro-basaltic melt. Geochimica et Cosmochimica Acta, 69 (21), 5071–5085.

10) Brounce, M., Kelley, K.A., and Cottrell, E. (2014) Fe3+/ΣFe variations in Mariana arc basalts and primary fO2 of the mantle wedge. Journal of Petrology, 55, 2513–2536.

11) Brounce, M., Kelley, K.A., Stern, R., Martinez, F., and Cottrell, E. (2016) The Fina Nagu volcanic complex: Unusual submarine arc volcanism in the rapidly deforming southern Mariana margin. Geochemistry, Geophysics, Geosystems, 17, 4078–4091.

12) Brounce, M., Stolper, E. and Eiler, J. (2017) Redox variations in Mauna Kea lavas, the oxygen fugacity of the Hawaiian plume, and the role of volcanic gases in Earth's oxygenation. Proceedings of the National Academy of Sciences of the USA, 114 (34), 8997-9002.

13) Bucholz, C.E., Gaetani, G.A., Behn, M.D., Shimizu, N. (2013) Post-entrapment modification of volatiles and oxygen fugacity in olivine-hosted melt inclusions. Earth and Planetary Science Letters, 374, 145–155.

14) Burnham, C.W. (1975) Water and magmas; a mixing model. Geochimica et Cosmochimica Acta, 39, 1077–1084.

15) Burnham, C.W. (1979) The importance of volatile constituents. In: Yoder, H.S. (Ed.), The Evolution of the Igneous Rocks. Princeton University Press, Princeton, NJ, pp. 439–482.

16) Canil, D. (1997) Vanadium partitioning and the oxidation state of Archean komatiite magmas. Nature 389, 842–845.

17) Canil, D. (1999) Vanadium partitioning between orthopyroxene spinel and silicate melt and the redox states of mantle source regions for primary magmas. Geochimica et Cosmochimica Acta, 63, 557-572.

18) Canil, D. and Fedortchouk, Y. (2001) Olivine-liquid partitioning of vanadium and other trace elements, with applications to modern and ancient picrites. Canadian Mineralogist, 39, 319-330.

19) Carmichael, I.S.E. (1991) The redox states of basic and silicic magmas: a reflection of their source regions? Contributions to Mineralogy and Petrology, 106, 129–141.

20) Chashchin, A.A., Martynov, Yu.A., Perepelov, A.B., Ekimova, N.I., and Vladimirova, T.P. (2011) Physical and chemical conditions of the formation and evolution of Late Pleistocene–Holocene magmas of the Gorely and Mutnovsky volcanoes, Southern Kamchatka. Russian Journal of Pacific Geology, 5 (4), 348–367 (translated from Tikhookeanskaya Geologiya, 30 (4), 87–108, 2011).

21) Cottrell, E., and Kelley, K.A. (2011) The oxidation state of Fe in MORB glasses and the oxygen fugacity of the upper mantle. Earth and Planetary Science Letters, 305, 270–282.

22) Cottrell, E., Kelley, K.A., Lanzirotti, A., and Fischer, R.A. (2009) High-precision determination of iron oxidation state in silicate glasses using XANES. Chemical Geology, 268, 167–179.

23) Danyushevsky, L., McNeill, A.W., and Sobolev, A.V. (2002) Experimental and petrological studies of melt inclusions in phenocrysts from mantle-derived magmas: an overview of techniques, advantages and complications. Chemical Geology,183, 5–24.

24) Danyushevsky, L.V. and Plechov, P.Yu. (2011) Petrolog3: Integrated software for modeling crystallization processes. Geochemistry, Geophysics, Geosystems, 12, Q07021

25) Deer, W.A., Howie, R.A., and Zussman, J. (1992) An introduction to the rock-forming minerals, 696 p. Longman Scientific & Technical, Harlow, England.

26) Duggen, S., Portnyagin, M., Baker, J., Ulfbeck, D., Hoernle, K., Garbe-Schönberg, D., and Grassineau, N. (2007) Drastic shift in lava geochemistry in the volcanic-front to rear-arc region of the Southern Kamchatkan subduction zone: Evidence for the transition from slab surface dehydration to sediment melting. Geochimica et Cosmochimica Acta, 71, 452-480.

27) Evans, K.A. (2012) The redox budget of subduction zones. Earth-Science Reviews, 113, 11–32

28) Ford, C.E., Russel, D.G., Craven, J.A., and Fisk, M.R. (1983) Olivine–liquid equilibria: temperature, pressure and composition dependence of the crystal/liquid cation partition coefficients for Mg, Fe^{2+}, Ca and Mn. Journal of Petrology, 24, 256–265.

29) Gaetani, G.A., and Grove, T.L. (1997) Partitioning of moderately siderophile elements among olivine, silicate melt and sulfide melts: Constraints on core formation on the Earth and Mars. Geochimica et Cosmochimica Acta, 32, 1057–1086.

30) Gaetani, G.A., O'Leary, J.A., Shimizu, N., Bucholz, C.E., and Newville, M. (2012) Rapid reequilibration of H_2O and oxygen fugacity in olivine-hosted melt inclusions. Geology, 40, 915–918.

31) Garbe-Schönberg, D., and Müller, S. (2014) Nano-particulate pressed powder tablets for LA-ICP-MS. Journal of Analytical Atomic Spectrometry, 29, 990-1000.

32) Griffin W, Powell W, Pearson N, O'reilly S (2008) GLITTER: data reduction software for laser ablation ICP-MS. Laser Ablation-ICP-MS in the earth sciences Mineralogical association of Canada short course series 40:204-207

33) Jackson, S.E. (2008) LAMTRACE data reduction software for LA-ICP-MS. In P.Sylvester, Ed., Laser Ablation ICP-MS in the Earth Sciences: Current Practices and Outstanding

751 Issues, 40, p. 305–307. Short Course Series, Mineralogical Association of Canada,
752 Quebec.
753 34) Jarosewich, E., Nelen, J.A., and Norberg, J.A. (1980) Reference samples for electron
754 microprobe analysis. Geostandards Newsletter, 4, 43-47.
755 35) Jochum, K.P., Stoll, B., Herwig, K., Willbold, M., Hofmann, A.W., Amini, M., Aarburg, S.,
756 Abouchami, W., Hellebrand, E., Mocek, B., and others (2006) MPI-DING reference
757 glasses for in situ microanalysis: New reference values for element concentrations and
758 isotope ratios. Geochemistry, Geophysics, Geosystems, 7. doi:10.1029/2005GC001060.
759 36) Jochum, K.P., Weis, U., Stoll, B., Kuzmin, D., Yang, Q., Raczek, I., Jacob, D.E., Stracke, A.,
760 Birbaum, K., Frick, D.A. (2011) Determination of reference values for NIST SRM 610–617
761 glasses following ISO guidelines. Geostandards and Geoanalytical Research, 35 (4), 397–
762 429.
763 37) Kelemen, P.B., and Holbrook, W.S. (1995) Origin of thick, high-velocity igneous crust
764 along the U.S. East Coast Margin, Journal of Geophysical Research, 100.
765 38) Kelley, K.A., and Cottrell, E. (2009) Water and the oxidation state of subduction zone
766 magmas. Science, 325, 605–607.
767 39) Kelley, K.A., and Cottrell, E. (2012) The influence of magmatic differentiation on the
768 oxidation state of Fe in a basaltic arc magma. Earth and Planetary Science Letters, 329–
769 330, 109–121.
770 40) Kress, V.C. and Carmichael, I.S.E. (1991) The compressibility of silicate liquids containing
771 Fe2O3 and the effect of composition, temperature, oxygen fugacity and pressure on
772 their redox states. Contributions to Mineralogy and Petrology, 108, 82-92
773 41) Laubier M., Grove T.L., and Langmuir C.H. (2014) Trace element mineral/melt
774 partitioning for basaltic and basaltic andesitic melts: An experimental and laser ICP-MS

775 study with application to the oxidation state of mantle source regions. Earth and
776 Planetary Science Letters, 392, 265-278.
777 42) Lee, C.-T.A., Leeman, W.P., Canil D., and Li, Z.-X.A. (2005) Similar V/Sc systematic in
778 MORBs and arc basalts: implications for the oxygen fugacities of their mantle source
779 regions. Journal of Petrology, 46, 2313–2336.
780 43) Lee, C.T.A., Luffi, P., Le Roux, V., Dasgupta, R., Albarede, F., and Leeman, W.P. (2010)
781 The redox state of arc mantle using Zn/Fe systematics. Nature, 468, 681–685.
782 44) Lee C-TA, Luffi P, Chin EJ, Bouchet R, Dasgupta R, Morton DM, Le Roux V, Yin Q-z, Jin D
783 (2012) Copper Systematics in Arc Magmas and Implications for Crust-Mantle
784 Differentiation. Science 336(6077):64-68 doi:10.1126/science.1217313
785 45) Mallmann, G., and O'Neill, H.St.C. (2009) The crystal/melt partitioning of V during
786 mantle melting as a function of oxygen fugacity compared with some other elements
787 (Al, P, Ca, Sc, Ti, Cr, Fe, Ga, Y, Zr and Nb). Journal of Petrology, 50, 1765-1794.
788 46) Mallmann, G., and O'Neill, H.St.C. (2013) Calibration of an empirical thermometer and
789 oxybarometer based on the partitioning of Sc, Y and V between olivine and silicate melt.
790 Journal of Petrology, 54 (5), 933-949.
791 47) Manzini, M., Bouvier, A.S., Baumgartner, L.P., Müntener, O., Rose-Koga, E.F., Schiano, P.,
792 Escrig, S., Meibom, A. and Shimizu, N. (2017) Weekly to monthly time scale of melt
793 inclusion entrapment prior to eruption recorded by phosphorus distribution in olivine
794 from mid-ocean ridges. Geology, doi: 10.1130/G39463.39461.
795 48) Moussallam Y, Oppenheimer C, Scaillet B, Gaillard F, Kyle P, Peters N, Hartley M, Berlo K,
796 Donovan A (2014) Tracking the changing oxidation state of Erebus magmas, from mantle
797 to surface, driven by magma ascent and degassing. Earth Planet Sci Lett 393(0):200-209
798 doi: 10.1016/j.epsl.2014.02.055

799 49) Mironov, N., Portnyagin, M., Botcharnikov, R., Gurenko, A., Hoernle, K., and Holtz, Fr.
800 (2015) Quantification of the CO_2 budget and H_2O–CO_2 systematics in subduction-zone
801 magmas through the experimental hydration of melt inclusions in olivine at high H2O
802 pressure. Earth and Planetary Science Letters, 425, 1–11.
803 50) Mungall, J.E. (2002) Roasting the mantle: Slab melting and the genesis of major Au and
804 Au-rich Cu deposits. Geology, 30(10), 915-918.
805 51) Newcombe, M. E., Fabbrizio, A. Y. Zhang, Ma, C. Le Voyer, M. Guan, Y., Eiler, J.M., Saal,
806 A.E. and Stolper, E.M. (2014) Chemical zonation in olivine-hosted melt inclusions.
807 Contributions to Mineralogy and Petrology, 168, 1030.
808 52) Nikolaev, G.S., Ariskin, A.A., Barmina G.S., Nazarova, M.A., and Almeev, R.R. (2016) Test
809 of the Ballhaus–Berry–Green Ol–Opx–Sp oxybarometer and calibration of a new
810 equation for estimating the redox state of melts saturated with olivine and spinel.
811 Geochemistry International, 54 (4), 301–320 (translated from Geokhimiya, 4, 323-343,
812 2016).
813 53) Papike, J.J., Burger, P.V., Bell, A.S., Le, L., Shearer, C.K., Sutton, S.R., Jones, J., and
814 Newville, M. (2013) Developing vanadium valence state oxybarometers (spinel-melt,
815 olivine-melt, spinel-olivine) and V/(Cr+Al) partitioning (spinel-melt) for martian olivine-
816 phyric basalts. American Mineralogist, 98, 2193-2196.
817 54) Papike, J.J., Karner, J.M., and Shearer, C.K. (2005) Comparative Planetary Mineralogy:
818 Valence State Partitioning of Cr, Fe, Ti, and V among Crystallographic Sites in Olivine,
819 Pyroxene, and Spinel from Planetary Basalts. American Mineralogist, 90, 277–290.
820 55) Parkinson, I.J., and Arculus, R.J. (1999) The redox state of subduction zones: insights
821 from arc-peridotites. Chemical Geology, 160, 409–423.

56) Pettke T, Halter WE, Webster JD, Aigner-Torres M, Heinrich CA (2004) Accurate quantification of melt inclusion chemistry by LA-ICPMS: a comparison with EMP and SIMS and advantages and possible limitations of these methods. Lithos 78(4):333-361

57) Plank, T., and Langmuir, C.H. (1988) An evaluation of the global variations in the major element chemistry of arc basalts, Earth and Planetary Science Letters, 90, 349–370.

58) Ponomareva V, Portnyagin M, Pendea IF, Zelenin E, Bourgeois J, Pinegina T, Kozhurin A (2017) A full Holocene tephrochronology for the Kamchatsky Peninsula region: applications from Kamchatka to North America. Quaternary Science Reviews 168:101-122, http://dx.doi.org/110.1016/j.quascirev.2017.1004.1031

59) Portnyagin, M., Almeev, R., Matveev, S., and Holtz, F. (2008) Experimental evidence for rapid water exchange between melt inclusions in olivine and host magma. Earth and Planetary Science Letters, 272, 541–552.

60) Portnyagin, M.V., Hoernle, K., Plechov, P.Y., Mironov, N.L., and Khubunaya, S.A. (2007) Constraints on mantle melting and composition and nature of slab components in volcanic arcs from volatiles (H_2O, S, Cl, F) and trace elements in melt inclusions from the Kamchatka Arc. Earth and Planetary Science Letters, 255, 53–69.

61) Qin, Z., Lu, F., and Anderson, A.T. Jr. (1992) Diffusive reequilibration of melt and fluid inclusions. American Mineralogist, 77, 565–576.

62) Ruscitto D.M., Wallace P.J., Johnson E.R., Kent A.J.R., and Bindeman, I.N. (2010) Volatile contents of mafic magmas from cinder cones in the Central Oregon High Cascades: implications for magma formation and mantle conditions in a hot arc. Earth and Planetary Science Letters, 298, 153–161.

63) Schuessler, J.A., Botcharnikov, R.E., Behrens, H., Misiti, V., and Freda, C. (2008) Oxidation state of iron in hydrous phono-tephritic melts. American Mineralogist, 93, 1493–1504.

64) Selyangin, O. B. (1993) New data on Mutnovsky volcano: Structure, evolution and prediction. Volcanology and Seismology, 15, 17-38 (translated from Vulkanologiya I Seysmologiya, 1, 17-35, 1993 (in Russian).

65) Shannon R (1976) Revised effective ionic radii and systematic studies of interatomic distances in halides and chalcogenides. Acta Crystallographica Section A 32(5):751-767 doi:doi:10.1107/S0567739476001551

66) Shearer, C.K., McKay, G., Papike, J.J., and Karner, J.M. (2006) Valence state partitioning of vanadium between olivine–liquid: Estimates of the oxygen fugacity of Y980459 and application to other olivine–phyric martian basalts. American Mineralogist, 91, 1657–1663.

67) Shishkina T.A. (2012) Storage conditions and degassing processes of low-K and high-Al tholeiitic island-arc magmas: Experimental constraints and natural observations for Mutnovsky volcano, Kamchatka//Leibniz University of Hannover, Germany. PhD Thesis. 214 pp.

68) Shishkina, T.A., Botcharnikov, R.E., Holtz, F., Almeev, R., Jazwa, A., and Jakubiak, A. (2014) Compositional and pressure effects on the solubility of H_2O and CO_2 in mafic melts. Chemical Geology, 388, 112-129.

69) Shishkina, T.A., Botcharnikov, R.E., Holtz, F., Almeev, R.R., Portnyagin, M. (2010) Solubility of H_2O and CO_2-bearing fluids in tholeiitic basalts at pressures up to 500 MPa. Chemical Geology, 277, 115-125.

70) Sisson, T. W., and Grove, T. L. (1993) Experimental investigations of the role of H_2O in calcalkaline differentiation and subduction zone magmatism. Contributions to Mineralogy and Petrology, 113, 143–166.

71) Sobolev, A.V., and Chaussidon, M. (1996) H_2O concentrations in primary melts from island arcs and mid-ocean ridges: implications for H_2O storage and recycling in the mantle. Earth and Planetary Science Letters, 137, 45–55.

72) Sobolev, A.V., Asafov, E.V., Gurenko, A.A., Arndt, N.T., Batanova, V.G., Portnyagin, M.V., Garbe-Schönberg, D., and Krasheninnikov, S.P. (2016) Komatiites reveal a hydrous Archaean deep-mantle reservoir. Nature, 531, 628-632.

73) Spandler, C., and O'Neill, H.St.C. (2010) Diffusion and partition coefficients of minor and trace elements in San Carlos olivine at 1300°C with some geochemical implications. Contributions to Mineralogy and Petrology, 159, 791–818.

74) Toplis, M. J. (2005) The thermodynamics of iron and magnesium partitioning between olivine and liquid: criteria for assessing and predicting equilibrium in natural and experimental systems. Contributions to Mineralogy and Petrology, 149, 22–39.

75) Tuff, J., and O'Neill, H.St.C. (2010) The effect of sulfur on the partitioning of Ni and other first-row transition elements between olivine and silicate melt. Geochimica et Cosmochimica Acta, 74, 6180-6205.

76) Wallace, P. (2005) Volatiles in subduction zone magmas: concentrations and fluxes based on melt inclusion and volcanic gas data. Journal of Volcanology and Geothermal Research, 140, 217-240.

77) Wilson, S.A. (1997) The collection, preparation, and testing of USGS reference material BCR-2, Columbia River, basalt. U.S. Geological Survey Open-File Report 98-00x, 45 p. Denver, Colo.

FIGURE CAPTIONS

Fig. 1. Comparison of published data on vanadium partitioning between olivine and melt and data from this study.

(a) D_V^{Ol-M} vs. ΔQFM variations in the experiments on vanadium partitioning between olivine and melt with selected area presented on Fig. 1b. (b) D_V^{Ol-M} vs. ΔQFM variations in the experiments on vanadium partitioning between olivine and melt performed at redox conditions at -5.0 < ΔQFM < +5.0. (c) Temperature (T in °C) vs. redox conditions (oxygen fugacity expressed in log10 units relative to the quartz-fayalite-magnetite buffer, ΔQFM) of the experiments on vanadium partitioning between olivine and silicate melt. (d) MgO vs. SiO_2 (wt.%) oxides concentrations in quenched glasses in equilibrium with olivine in run products of the vanadium partitioning experiments. Data from this study are shown with red circles and grey area. Different symbols show data from the previously published experiments (see legend): Gaetani and Grove, 1997; Canil, 1997; 1999; Canil and Fedortchouk, 2001; Shearer et al., 2006; Mallmann and O'Neill, 2009; 2013; Tuff and O'Neill, 2010; Papike et al., 2013; Laubier et al., 2014. The compositions of natural melt inclusions in olivines from Mutnovsky basalts are shown by crossed symbols (NH – not-heated, RH – re-heated in the experiment) on Fig. 1d. The yellow star shows the composition of Mutnovsky basalt (sample #N72) used as a starting composition for the experiments of this study.

Fig. 2. Optical and back-scattered electron-images of the studied experimental and natural samples.

(a-b) Optical and back-scattered electron-images of the experimental products of run V8 (0.3 GPa, 1030°C). Run products in "V"-series are presented by relatively large subidiomorphic olivine crystals (size up to 200 μm) surrounded by quenched basaltic glass. Some olivine grains contain glassy inclusions. Tiny grains of magnetite are distributed in glass and as inclusions in olivine. (c-e) Back-scattered electron-images of the experimental products of "N"-series: runs

N86 (0.1 GPa, 1075°C), N69 (0.3GPa, 1025°C) and N33 (0.3GPa, 1150°C). Olivines in run products of "N"-series are subidiomorphic and have smaller size (up to 50 μm) than in "V"-series and usually contain poikilitic inclusions of plagioclase and rarely magnetite. In some runs small (size up to 15 μm) isometric CPx-crystals are observed. (f) Naturally quenched melt inclusion in an olivine from Mutnovsky tephra with holes from LA-ICP-MS.

Fig. 3. Results of analysis of small olivine crystals after experiments of "N"-series by LA-ICP-MS.

(a) Intensities (cps) of some elements (Mg, Al, V, Ti, Ba) versus ablation time (sec) measured by LA-ICP-MS in a small grain of olivine in the experiment N86. Spectra show the entrapment of various phases (olivine, plagioclase and glass) by the laser spot during the analysis.

(b) Forecast estimation of vanadium content in experimental olivines applied to run N72-Cr3-45 in this study. Various amounts of matrix glass were captured by the laser beam during the LA-ICP-MS analyses because of the small size of olivine grains in run products of "N"-series and common melt inclusions, which lead to overestimated V and Al concentrations for olivine. The real concentrations of vanadium (or other trace elements) in olivine were performed by plotting the data against Al content and extrapolating them to 100 ppm Al as estimated from the EMPA analyses of big olivine grains from "V"-series. 8-10 points were used to calculated average olivine composition in every run.

Fig. 4. Partitioning of V between olivine and melt obtained in this study.

(a) Vanadium concentrations in experimentally produced coexisting olivine and melt in comparison with the compositions of melt inclusions in olivine from Mutnovsky volcano (filled grey square); (B) $D_V^{Ol\text{-}M}$ vs. ΔQFM variations in the experiments on vanadium partitioning

943 performed at redox conditions of -5.0 < ΔQFM < +5.0. Data from this study are shown with red
944 circles, previously published data - with crosses (literature data are the same as in Fig. 1). Fig.
945 4b also shows the equations 1 and 2 derived in this study as a linear function of the
946 dependence between D_V^{Ol-M} and ΔQFM for 12 olivine-melt partitioning experiments with
947 Mutnovsky basalt (solid black line) with dashed lines representing the 95% interval of
948 confidence for the calibrated equation. The dotted line on Fig. 4-b represents the trend of the
949 D_V^{Ol-M} vs. ΔQFM dependence according to the equation derived for komatiites in Canil and
950 Fedortchouk (2001). Grey squares are the results of calculation of ΔQFM from D_V^{Ol-M} and melt
951 and olivine compositions obtained in the experiments from this study for Mutnovsky basalt
952 using the empirical equation from Mallmann and O'Neill (2013).
953
954 **Fig. 5.** Calibration of V-in-olivine oxybarometer for low-Temperature conditions.
955 (a) D_V^{Ol-M} vs. ΔQFM variations in the experiments on vanadium partitioning between
956 olivine and melt from this study and previously published in the range of redox conditions of -
957 5.0 < ΔQFM < +5.0 (the list of references is the same as for Fig. 1). Different symbols represent
958 experiments performed within a certain interval of temperatures (see legend). We can note a
959 general negative effect of temperature on D_V^{Ol-M} values at the same ΔQFM (i.e., lower-
960 temperature experiments derive higher values of D_V^{Ol-M}).
961 (B) D_V^{Ol-M} vs. ΔQFM variations in the experiments on vanadium partitioning between
962 olivine and melt performed at redox conditions in the range of -5.0 < ΔQFM < +5.0. Data from
963 this study are shown with red circles, from previously published data - with crossed symbols
964 (the list of references is the same as for Fig. 1). Grey circles represent experiments from the
965 literature performed at temperature below 1250°C, which were used in this study for the
966 calibration of equations (3) and (4). White circles are published experiments performed at
967 temperature below 1250°C, which were rejected from the calibration of equations (3) and (4).

The rejected experiments include: 2 groups of runs from Mallmann and O`Neill (2013) performed at 1245°C, redox conditions of QFM+0.11 and QFM -2.85 with glasses containing more than 10 wt.% Na_2O, which have much lower $D_V^{Ol\text{-}M}$ at the same fO_2 in comparison to other experiments performed at T<1250°C at the same redox conditions. The other experiments performed at T< 1250°C selected for calibration have less than 4 wt.% Na_2O in melt. Also rejected 3 data points from Papike et al. (2013) performed at 1200°C, ΔQFM of -2.54, -3.54 and – 4.54, which seemed to have a more flat slope of $D_V^{Ol\text{-}M}$ vs. ΔQFM dependence in comparison to the other experiments performed at T below 1250°C. On Fig. 5b the solid black line also shows the experimentally determined negative linear correlation of $D_V^{Ol\text{-}M}$ vs. ΔQFM for Mutnovsky basalt and the selected previously published experiments performed at temperatures ≤1250°C (59 datapoints including data from this study); dashed lines representing the 95% interval of confidence for the calibrated equation (3). Red solid line is the regression obtained for 12 runs with Mutnovsky basalt (eq.1). Dotted line shows the calibration of Canil and Fedortchouk (2001).

Fig. 6. Testing different formulations of V-in-oxybarometer to predict ΔQFM for low-T experiments. The test was performed for 59 olivine-melt pairs equilibrated at T<1250°C (this study; Canil, 1997; Canil and Fedorthouk, 2001; Mallmann and O`Neill, 2013; Papike et al., 2013; Laubier et al., 2014). The following equations were tested: 1) Equation (4) from this study, 2) equation by Canil and Fedortchouk (2001) and 3) equation from Mallmann and O`Neill (2013). Dashed lines represent the deviation from equiline of 0.25, 0.5 and 1.0 fO_2 log units.

Fig. 7. Comparison of redox conditions (ΔQFM) determined for Mutnovsky basalts using different oxybarometers. Oxibarometers using V partitioning between olivine and melt are from this study (equation 2), Canil and Fedortchouk (2001), Mallmann&O`Neill (2013); spinel-olivine oxybarometers are from Ballhaus et al. (1991) and Nikolaev et al. (2016).

This is a preprint, the final version is subject to change, of the American Mineralogist (MSA)
Cite as Authors (Year) Title. American Mineralogist, in press.
DOI: http://dx.doi.org/10.2138/am-2018-6210

992 **Fig. 8.** Modelling of V re-equilibration between melt inclusion and external magma. The
993 calculations are performed using model of Qin et al. (1992) for melt inclusion with diameter (d)
994 of 50 micron in the center of 1 mm olivine crystal for the case when the initial equilibrium has
995 changed at 1300°C and redox conditions corresponding QFM and QFM+2. V diffusivity (K_V) in
996 olivine at 1300°C is after Spandler et al. (2010). V partitioning between olivine and melt at
997 different redox conditions is after this study. The modeling results imply that 50% re-
998 equilibration of the inclusion will be achieved in about 1.5 years at QFM and in about 2 years at
999 QFM+2.

1000 **FIGURES for manuscript**

This is a preprint, the final version is subject to change, of the American Mineralogist (MSA)
Cite as Authors (Year) Title. American Mineralogist, in press.
DOI: http://dx.doi.org/10.2138/am-2018-6210

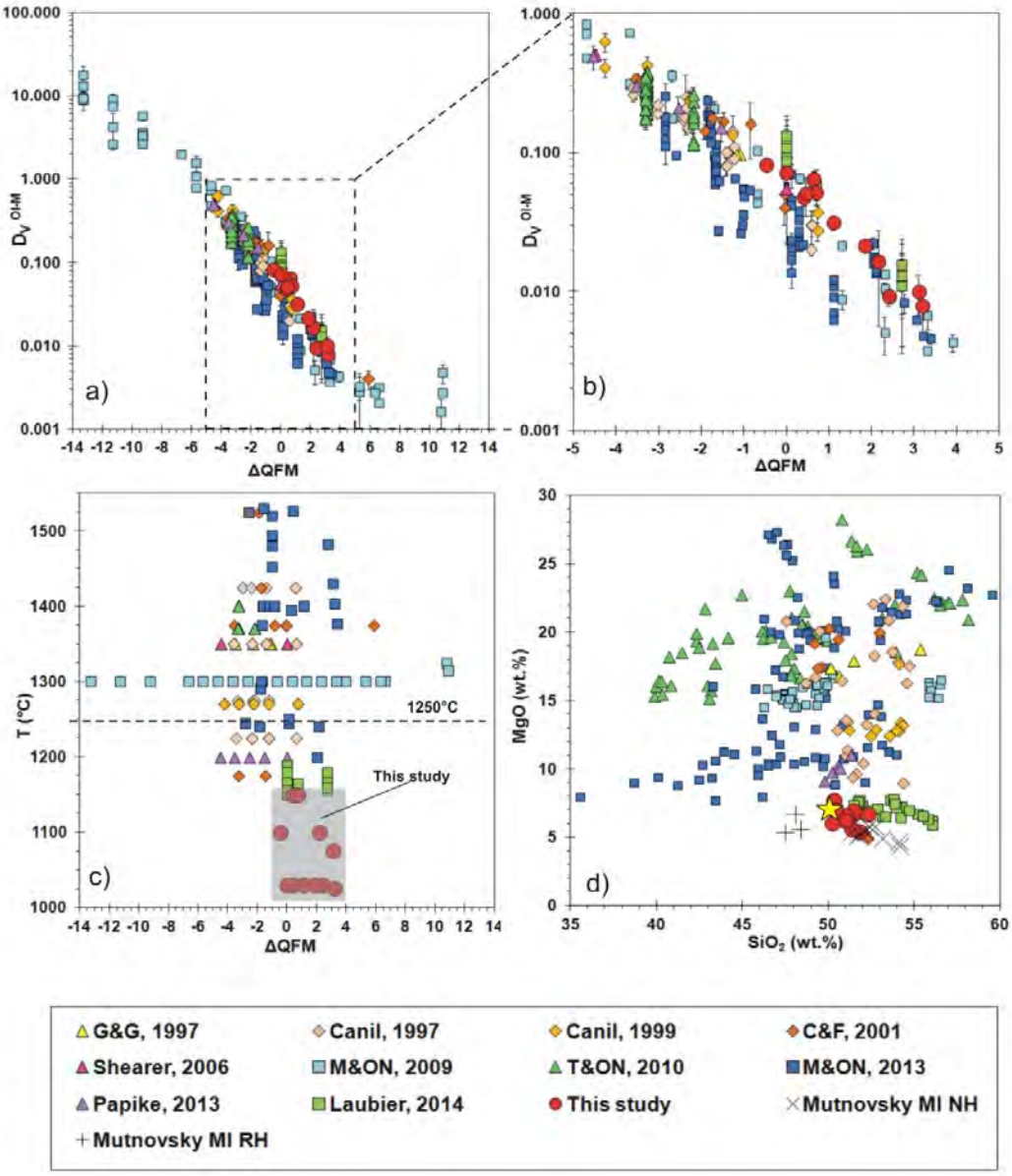

Fig. 1 a,b,c,d.

This is a preprint, the final version is subject to change, of the American Mineralogist (MSA)
Cite as Authors (Year) Title. American Mineralogist, in press.
DOI: http://dx.doi.org/10.2138/am-2018-6210

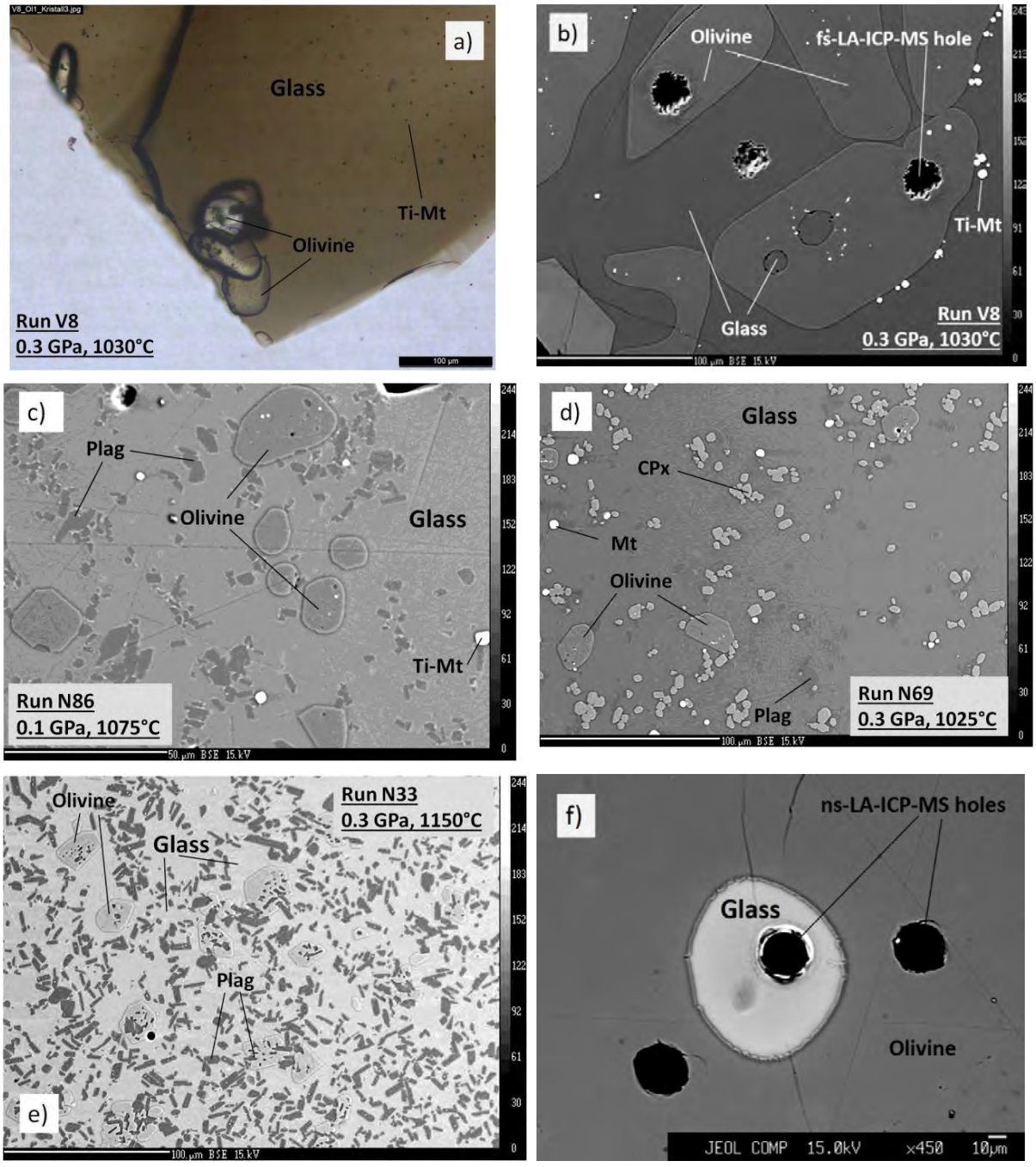

Fig. 2. a,b,c,d,e,f.

This is a preprint, the final version is subject to change, of the American Mineralogist (MSA)
Cite as Authors (Year) Title. American Mineralogist, in press.
DOI: http://dx.doi.org/10.2138/am-2018-6210

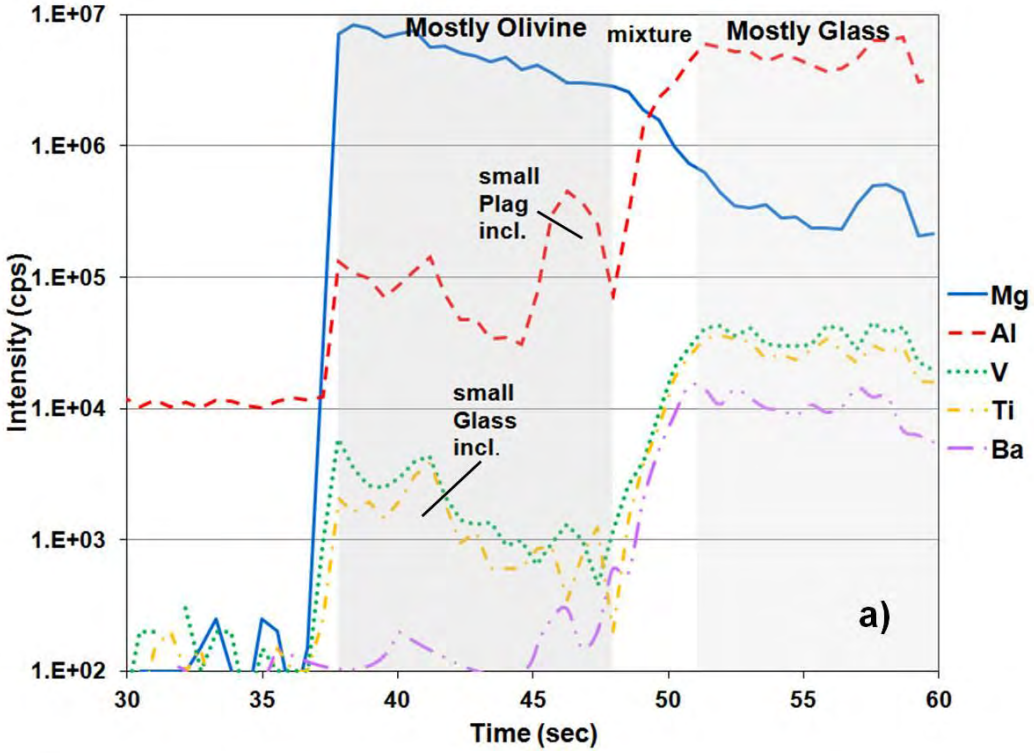

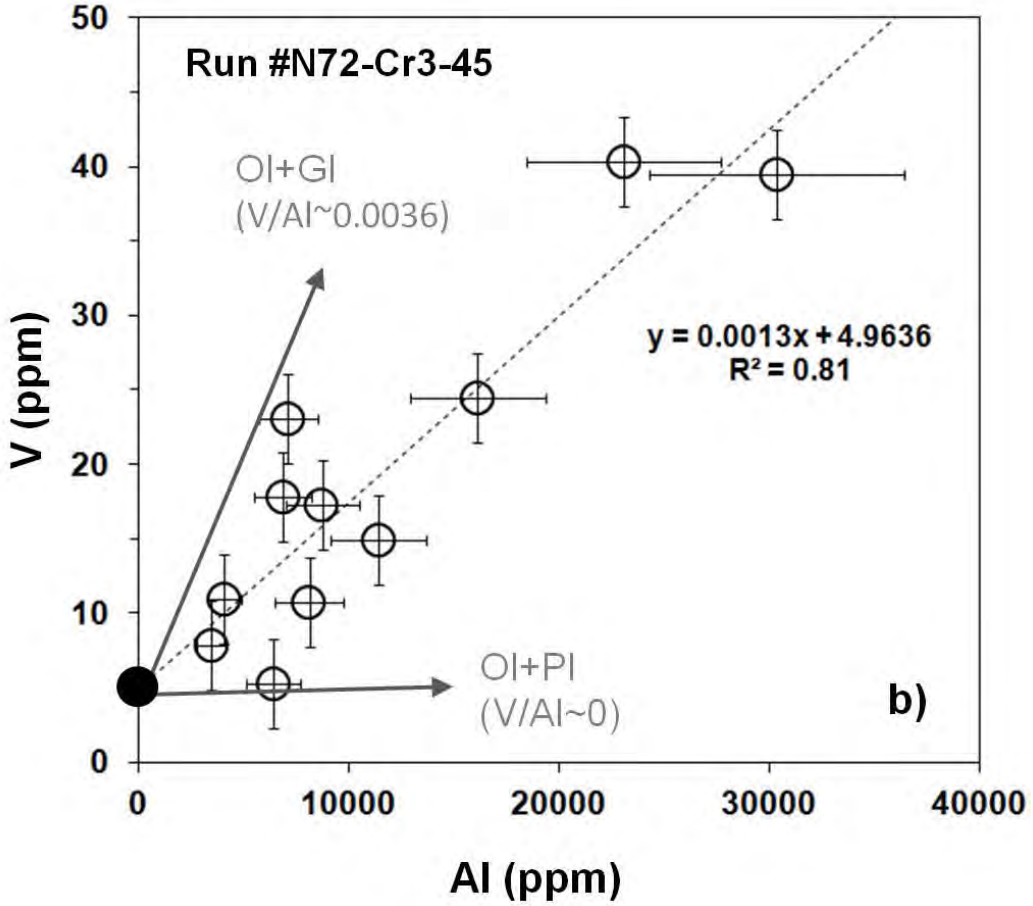

Fig. 3 a, b

This is a preprint, the final version is subject to change, of the American Mineralogist (MSA)
Cite as Authors (Year) Title. American Mineralogist, in press.
DOI: http://dx.doi.org/10.2138/am-2018-6210

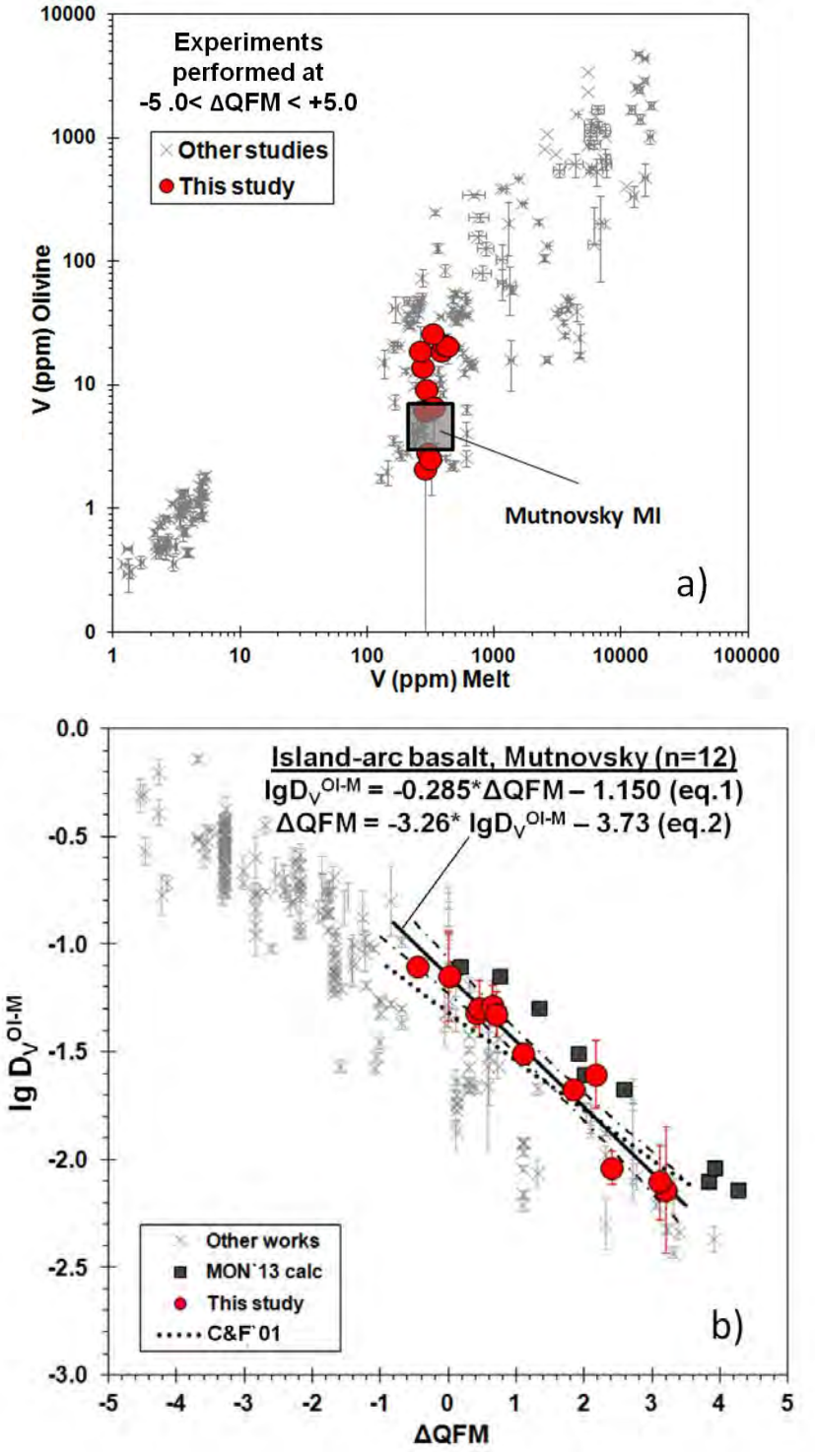

Fig. 4. a, b

This is a preprint, the final version is subject to change, of the American Mineralogist (MSA)
Cite as Authors (Year) Title. American Mineralogist, in press.
DOI: http://dx.doi.org/10.2138/am-2018-6210

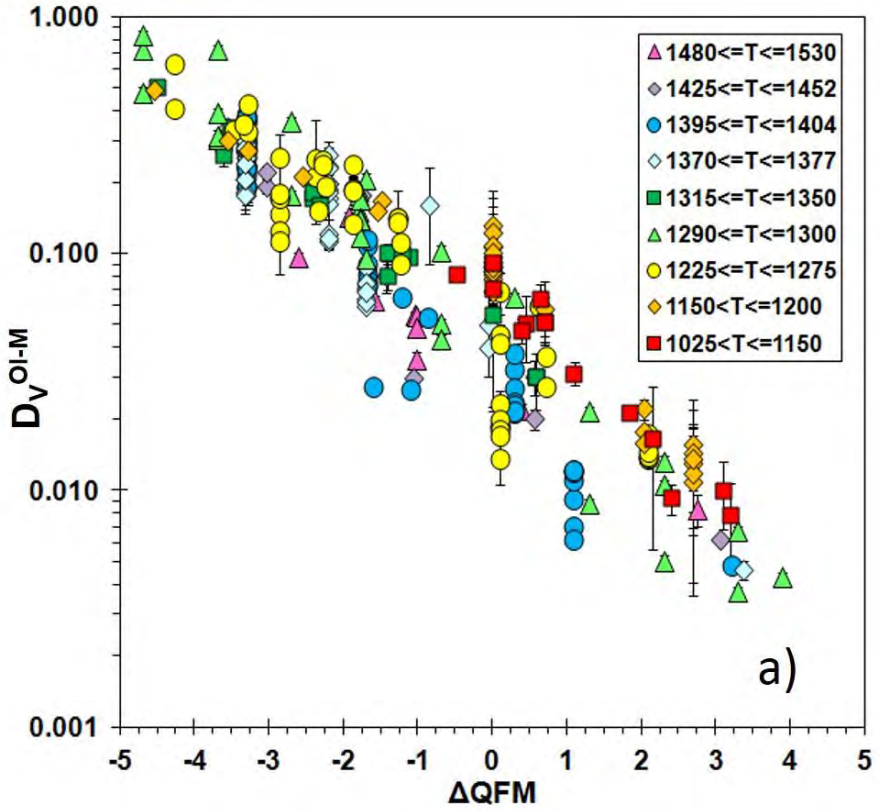

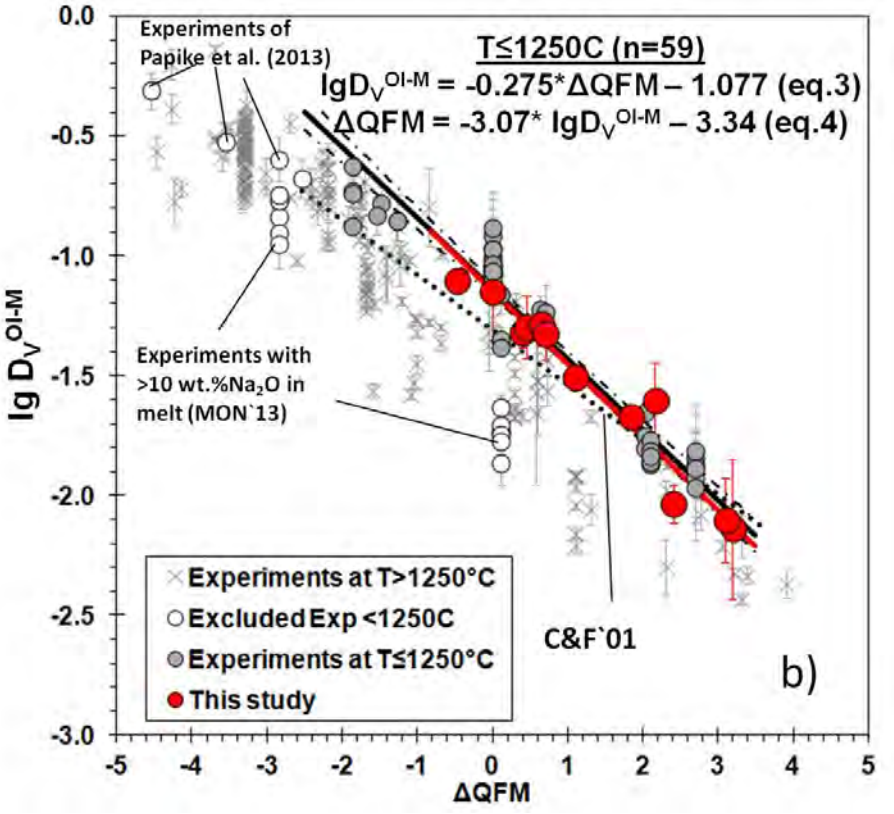

Fig. 5 a, b

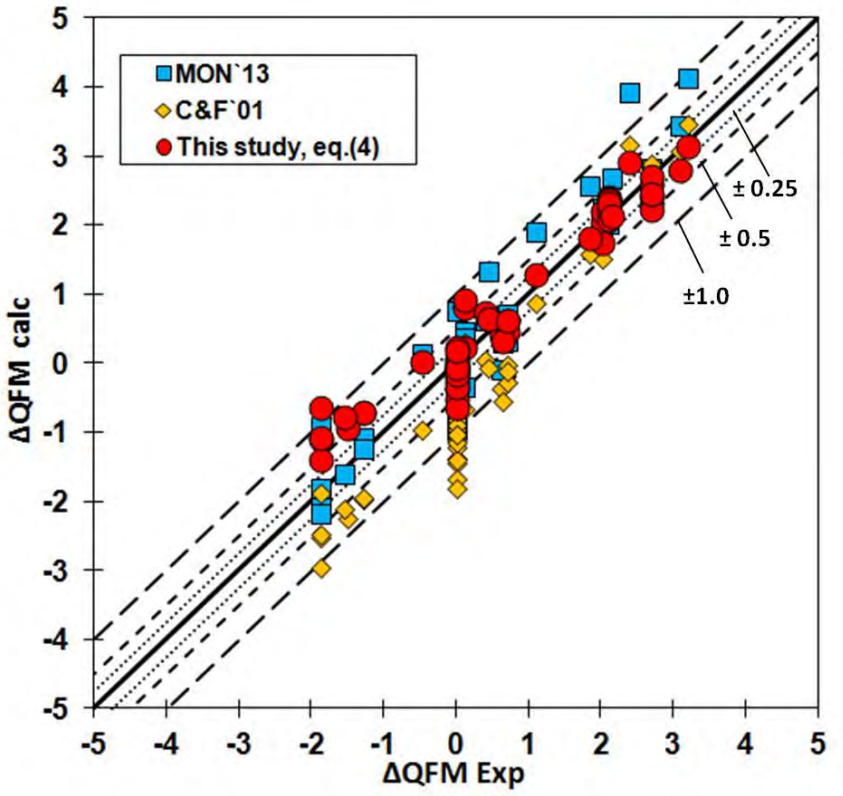
MON`13
C&F`01
This study, eq.(4)
± 0.25
± 0.5
±1.0
ΔQFM calc
ΔQFM Exp
5
4
3
2
1
0
-1
-2
-3
-4
-5

Fig. 6.

This is a preprint, the final version is subject to change, of the American Mineralogist (MSA)
Cite as Authors (Year) Title. American Mineralogist, in press.
DOI: http://dx.doi.org/10.2138/am-2018-6210

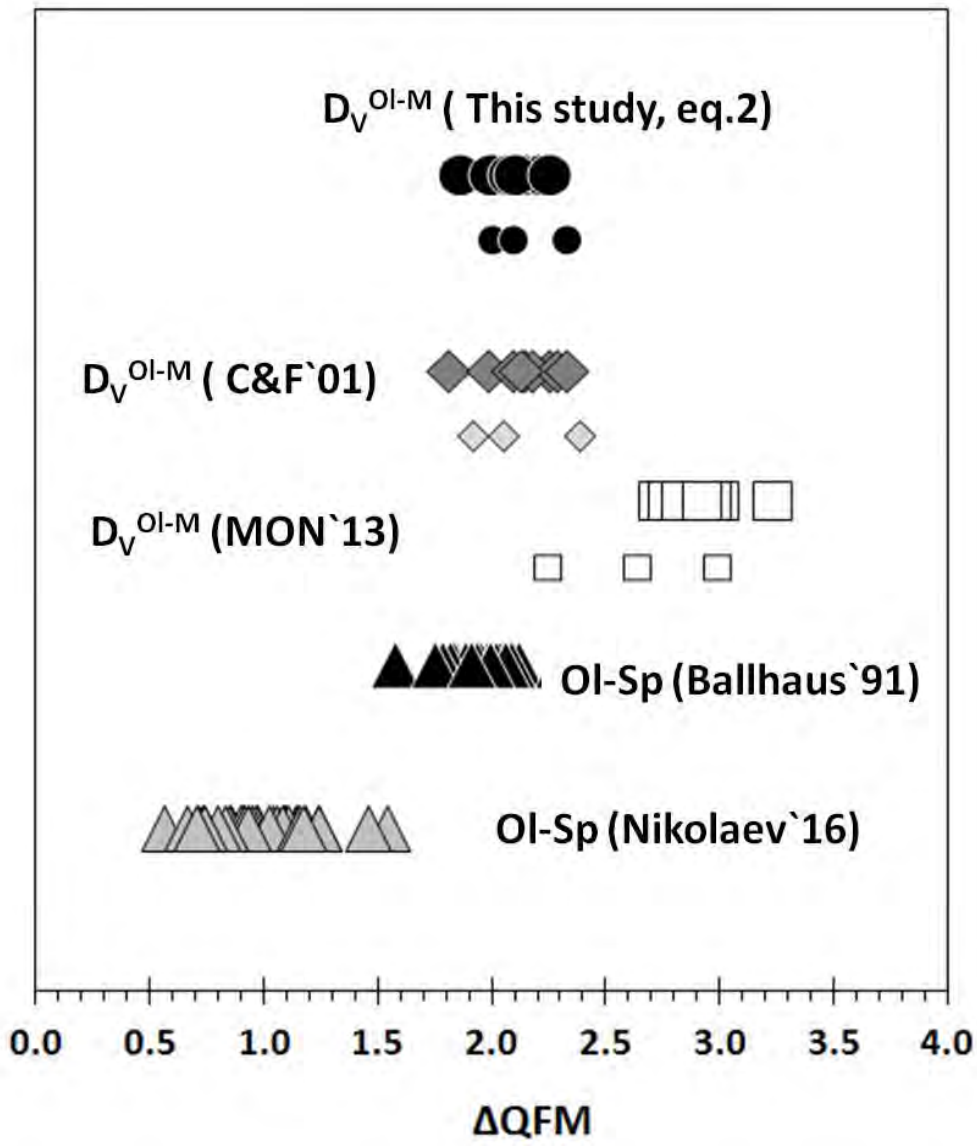

1034

1035 **Fig. 7**

This is a preprint, the final version is subject to change, of the American Mineralogist (MSA)
Cite as Authors (Year) Title. American Mineralogist, in press.
DOI: http://dx.doi.org/10.2138/am-2018-6210

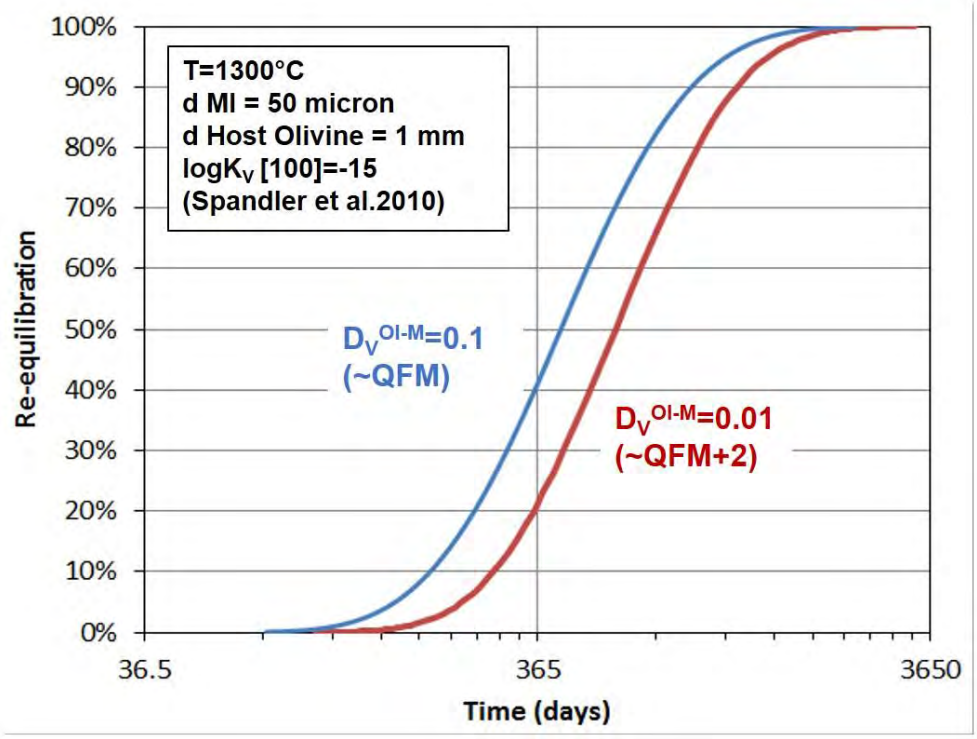

Fig. 8

Table 1. Experimental conditions and compositions of glasses and olivines in run products

Run #	N72-Cr3-5	N72-Cr3-33	N72-Cr3-34	N72-Cr3-45	N72-Cr3-60	N72-Cr3-69	N72-Cr1-86	V8	V13	V18	V25	V26
T, °C	1150	1150	1150	1100	1100	1025	1075	1030	1030	1030	1030	1030
P, MPa	300	300	300	300	300	300	100	303	320	303	285	294
t, h	3	15	15	15	15	73	72	72	92	95	72	72
ΔQFM	0.4	0.6	0.7	2.1	-0.5	3.2	3.1	1.1	0.5	0.0	2.4	1.8
CP	o,p	o,p,c	p,c	o,p	o,p	o,p,c,m	o,p,m	o,m	o,am*	o,am*	o,c,m	o,c,m
						Glass						
SiO2	50.6	51.3	51.6	51.4	52.3	51.0	50.4	50.5	51.8	51.4	51.0	50.2
TiO2	1.24	1.27	1.27	1.00	1.00	0.94	0.94	0.92	0.89	0.93	0.92	0.96
Al2O3	15.3	16.1	15.4	17.2	18.2	18.4	17.8	18.4	19.1	19.1	18.8	19.0
FeO	11.4	10.7	10.8	9.7	7.1	8.8	9.6	9.3	8.4	8.6	8.6	9.5
MnO	0.2	0.2	0.2	0.3	0.2	0.2	0.3	0.1	0.2	0.2	0.2	0.1
MgO	7.6	6.5	6.8	6.9	6.7	6.6	7.0	6.5	5.4	5.6	6.2	6.0
CaO	10.9	11.1	11.2	11.0	11.5	11.0	10.9	11.5	11.4	11.5	11.5	11.3

Na2O	2.4	2.5	2.4	2.2	2.7	2.7	2.8	2.4	2.4	2.4	2.5	2.5
K2O	0.28	0.32	0.35	0.24	0.28	0.25	0.25	0.24	0.27	0.27	0.25	0.27
Total	100	100	100	100	100	100	100	100	100	100	100	100
H_2O	0.6 (0.8)	0.7 (1.8)	0.8 (2.3)	2.1 (2.3)	2.5 (2.4)	5.3 (5.6)	2.9 (0.1)	6.3 (5.9)	6.3 (8.2)	6.3 (8.0)	6.3 (6.4)	6.3 (6.5)
V	391	403	431	309	329	289	317	293	277	263	303	292
2SE	(39)	(36)	(31)	(52)	(8)	(23)	(27)	(2)	(23)	(10)	(5)	(4)
						Olivine						
Fo EMP	80.9	80.3	80.6	83.8	84.0	83.8	84.9	81.2	80.7	80.2	83.0	81.4
Fo ICP	80.7	80.1	80.6	84.9	83.8	85.8	87.3	79.1	78.1	76.3	81.3	80.8
V (ns)	18.5	25.9	22.1	5.1	26.6	2.3	3.2	8.4	NA	NA	3.4	NA
2SE	(1.3)	(3.0)	(3.6)	(3.2)	(1.3)	(0.8)	(1.0)	(1.5)			(0.6)	
V (fs)	NA	NA	NA	NA	NA	NA	NA	9.1	14.0	18.7	2.8	6.2
2SE								(1.0)	(4.2)	(13.0)	(0.4)	(0.2)
$D_V^{Ol\text{-}M}$	0.047	0.064	0.051	0.016	0.081	0.008	0.010	0.031	0.050	0.071	0.009	0.021
2SE	(0.006)	(0.009)	(0.009)	(0.011)	(0.005)	(0.003)	(0.003)	(0.003)	(0.016)	(0.050)	(0.001)	(0.001)
Kd $_{Fe\text{-}Mg}^{Ol\text{-}M}$ (LA)	0.34	0.32	0.33	0.32	0.36	0.38	0.32	0.36	0.32	0.33	0.39	0.35
Kd $_{Fe\text{-}Mg}^{Ol\text{-}M}$ (EMP)	0.33	0.32	0.33	0.35	0.36	0.45	0.40	0.36	0.32	0.33	0.39	0.35

Notes for Table 1.

V content in olivines of N-series was calculated from measured values assuming 100 ppm Al in olivine (see description in text); (ns) and (fs) refer to nanosecond and femtosecond LA-systems, respectively. Uncertainties for V are 2 SE (standard error of mean, 95% confidence level) calculated as 2*1s/SQRT(n), where 1s is standard deviation and n is the number of analyzes. Uncertainty of D_V was calculated using a conventional rule for error propagation: $Error(X/Y) = X/Y*[(ErrorX/X)^2+(ErrorY/Y)^2)]^{0.5}$. NA – not analyzed in these samples.

Error of ΔQFM is estimated as ±0.3 lgfO_2 units for "N"-series and ±0.2 lgfO_2 for "V"-series.

Crystal phases (CP): o - olivine, p- plagioclase, c - clinopyroxene, m - magnetite, am* - quench amphibole.

EMPA glass analyzes are recalculated to 100% anhydrous total. H_2O contents were determined by FTIR for N-series and calculated from H_2O solubility data for Mutnovsky basalt (Shishkina et al., 2010) for H_2O-saturated runs of V-series. The H_2O values in brackets were

1055 determined by difference between EMPA total and 100%.

1056 The values of $Kd_{Fe2+-Mg}^{Ol-Melt}$ calculated using FeO and MgO contents calculated from LA-
1057 ICP-MS or EMP in olivines and EMP analyzes of glasses from the run products with Fe^{2+}
1058 estimated by the model of Kress and Carmichael (1991) (see Appendix-A1).

1059

1060

1061 **Table 2. Major and trace elements compositions of melt inclusions and host-olivines.**

Inclusion number	**Units**	**KM9-10-29-1**	**KM9-10-29-2**	**KM9-10-32-2**	**KM9-10-32-3**	**KM9-10-34-2**	**KM9-10-37-1**	**KM9-11-42-1**	**KM9-11-43-1**	**KM9-11-43-2**	**N72-5a**	**N72-8**	**N71-3a**
Re-heating		No	No	No	No	No	No	No	No	No	Yes	Yes	Yes
MI diameter	µm	110	45	75	140	45	100	100	127	75	78	70	63
Melt inclusions													
SiO2	wt%	53.15	53.38	51.16	50.94	51.16	51.77	51.94	50.55	52.41	46.66	47.24	47.54
TiO2	wt%	1.21	1.06	1.21	1.07	1.11	1.19	1.17	1.10	1.12	0.96	0.80	0.74
Al2O3	wt%	17.28	17.80	16.81	17.05	16.06	16.51	16.31	16.91	17.24	19.86	18.27	19.03
FeO	wt%	8.24	8.46	9.67	9.17	9.61	10.34	10.56	10.01	9.31	9.17	9.20	9.41
MnO	wt%	0.17	0.29	0.21	0.19	0.24	0.12	0.18	0.18	0.26	0.18	0.13	0.05
MgO	wt%	4.34	4.62	5.25	5.07	5.32	5.72	5.71	5.29	4.86	5.29	6.61	5.50
CaO	wt%	8.52	8.43	10.07	10.66	10.21	8.95	9.08	10.32	8.61	12.05	12.23	11.82
Na2O	wt%	3.98	3.49	3.39	3.39	3.51	3.26	2.61	3.13	3.55	3.13	2.86	3.44
K2O	wt%	0.80	0.79	0.50	0.47	0.54	0.61	0.53	0.50	0.71	0.47	0.46	0.35
P2O5	wt%	0.29	0.14	0.25	0.21	0.18	0.15	0.19	0.25	0.23	0.22	0.20	0.12
H2O	wt%	2.03	1.54	1.48	1.77	2.07	1.39	1.73	1.77	1.71	2.00	2.00	2.00
Total	wt%	100.00	100.00	100.00	100.00	100.00	100.00	100.00	100.00	100.00	100.00	100.00	100.00
V	ppm	295	276	370	370	348	283	365	354	395	462	285	288
Sc	ppm	33	36	44	45	41	41	45	47	36			
Y	ppm	21	17	22	22	21	29	24	22	21	26	20	21
Host olivine													
SiO2	wt%	39.09	39.16	39.12	38.70	38.55	38.55	38.30	38.24	38.80	38.36	39.05	38.51
Al2O3	wt%	0.02	0.02	0.03	0.03	0.02	0.02	0.02	0.02	0.03			
FeO	wt%	19.65	19.86	19.73	19.56	19.10	19.44	20.56	20.26	20.18	17.95	15.28	17.71
MnO	wt%	0.36	0.36	0.36	0.35	0.34	0.35	0.37	0.37	0.37	0.31	0.24	0.29
MgO	wt%	42.0	42.1	42.3	42.4	42.4	42.3	41.3	41.6	41.5	42.5	44.9	42.8

		8	8	8	5	8	2	6	5	5	7	5	1
CaO	wt%	0.19	0.18	0.22	0.23	0.21	0.18	0.22	0.20	0.19	0.18	0.17	0.18
Cr2O3	wt%	0.00	0.00	0.01	0.01	0.01	0.01	0.00	0.00	0.01	0.01	0.01	0.01
NiO	wt%	0.05	0.05	0.06	0.06	0.05	0.05	0.06	0.05	0.05	0.12	0.14	0.05
Total	wt%	101.44	101.80	101.90	101.38	100.75	100.90	100.90	100.80	101.17	99.50	99.84	99.57
Fo	mol%	79.2	79.1	79.3	79.5	79.8	79.5	78.2	78.6	78.6	80.9	84.0	81.2
V	ppm	5.7	4.9	6.0	5.6	5.5	4.2	6.1	5.8	5.8	6.6	5.2	4.9
Sc	ppm	8.8	8.4	9.5	8.8	9.4	8.6	10.4	9.8	9.4			
Y	ppm	0.118	0.081	0.102	0.084	0.107	0.129	0.142	0.088	0.104	0.102	0.073	0.073
Ol (%)		1.1	3.1	5.1	2.7	5.3	6.2	5.9	3.0	3.3	2.5	-4.3	-3.7
Calculated parameters													
T OL DRY (Ford`83)	°C	1123	1128	1130	1118	1135	1157	1147	1126	1134	1100	1156	1125
T OL H2O (Almeev'07)	°C	1057	1074	1077	1058	1067	1106	1088	1066	1075	1034	1090	1059
T Sc/Y (MON`13)	°C	1084	1078	1080	1062	1087	1092	1129	1057	1062			
D_V^{Ol-M}		0.019	0.018	0.016	0.015	0.016	0.015	0.017	0.016	0.015	0.014	0.018	0.017
ΔQFM (MON`13)		2.7	3.0	2.8	3.0	2.8	3.0	2.8	2.9	3.2	3.0	2.2	2.6
ΔQFM (C&F`01)		1.8	2.0	2.1	2.3	2.2	2.3	2.1	2.1	2.3	2.4	1.9	2.0
ΔQFM (TS, eq.2)		1.8	1.9	2.0	2.2	2.1	2.1	2.0	2.1	2.2	2.3	2.0	2.1
ΔQFM (TS, eq.4)		1.9	2.0	2.1	2.2	2.1	2.2	2.0	2.1	2.2	2.3	2.1	2.1

Notes for Table 2.

Melt inclusion compositions were recalculated to equilibrium with host olivine in PETROLOG3 (Danyushevsky, Plechov, 2011) as explained in text. Compositions of melt inclusion glasses measured by EMPA (major elements), SIMS (H_2O) and ns-LA-ICP-MS (V, Sc, Y) are given in Appendix A1. Initial H_2O in reheated inclusions was assumed to equal to 2%. Ol(%) is amount of host-olivine required to add (+) or remove (-) from a measured melt inclusion composition (Appendix-A1) to reconstruct the equilibrium melt composition with the host-olivine.

Calculated parameters: T Ol DRY - unhydrous liquidus temperature of olivine by Ford et al. (1983); T Ol wet - liquidus olivine temperature corrected for the presence of H_2O in melt by

Almeev et al. (2007); T Sc/Y - equilibrium temperature calculated from Sc and Y partitioning between olivine and melt (Mallmann and O`Neill, 2013); ΔQFM are calculated from V partitioning between olivine and melt using the equations from Mallmann and O`Neill (2013) (MON`13), Canil and Fedortchouk (2001) (C&F`01), and equations 2 and 4 from this study (TS, eq.2, 4).